

# Accepted Manuscript

Synthesis and evaluation of 7-substituted coumarin derivatives as multimodal monoamine oxidase-B and cholinesterase inhibitors for the treatment of Alzheimer's disease

Jacques Joubert, Germaine B. Foka, Benjamin P. Repsold, Douglas W. Oliver, Erika Kapp, Sarel F. Malan

PII: S0223-5234(16)30772-3

DOI: [10.1016/j.ejmech.2016.09.041](https://doi.org/10.1016/j.ejmech.2016.09.041)

Reference: EJMECH 8907

To appear in: *European Journal of Medicinal Chemistry*

Received Date: 28 July 2016

Revised Date: 12 September 2016

Accepted Date: 13 September 2016

Please cite this article as: J. Joubert, G.B. Foka, B.P. Repsold, D.W. Oliver, E. Kapp, S.F. Malan, Synthesis and evaluation of 7-substituted coumarin derivatives as multimodal monoamine oxidase-B and cholinesterase inhibitors for the treatment of Alzheimer's disease, *European Journal of Medicinal Chemistry* (2016), doi: 10.1016/j.ejmech.2016.09.041.

This is a PDF file of an unedited manuscript that has been accepted for publication. As a service to our customers we are providing this early version of the manuscript. The manuscript will undergo copyediting, typesetting, and review of the resulting proof before it is published in its final form. Please note that during the production process errors may be discovered which could affect the content, and all legal disclaimers that apply to the journal pertain.



# Synthesis and evaluation of 7-substituted coumarin derivatives as multimodal monoamine oxidase-B and cholinesterase inhibitors for the treatment of Alzheimer's disease

Jacques Joubert<sup>a,\*</sup>, Germaine B. Foka<sup>a</sup>, Benjamin P. Repsold<sup>b</sup>, Douglas W. Oliver<sup>b</sup>, Erika Kapp<sup>a</sup>, Sarel F. Malan<sup>a</sup>

<sup>a</sup>Pharmaceutical Chemistry, School of Pharmacy, University of the Western Cape, Private Bag X17, Bellville, South Africa. <sup>b</sup>School of Pharmacy, North-West University, Private Bag X6001, Potchefstroom, South Africa

\*Corresponding author at present address: School of Pharmacy, University of the Western Cape, Private Bag X17, Bellville 7535, South Africa. Tel: +27 21959 2195; e-mail: [jjoubert@uwc.ac.za](mailto:jjoubert@uwc.ac.za)

---

## Abstract:

A series of 7-substituted coumarin derivatives were designed and synthesised to display ChE and MAO-B inhibitory activity. The compounds consisted out of a coumarin structure (MAO-B inhibitor) and benzyl-, piperidine-, *N*-benzylpiperidine- or *p*-bromo-*N*-benzylpiperazine moieties, resembling the *N*-benzylpiperidine function of donepezil (ChE inhibitor), connected via an alkyl ether linkage at the 7 position. The biological assay results indicated that all the compounds (**1-25**) displayed selective inhibition to hMAO-B over hMAO-A, with the benzyloxy series (**1-8**, **10-13**) showing nano-molar hMAO-B inhibition (IC<sub>50</sub>: 0.5 – 73 nM). Limited ChE inhibitory activity was however observed for the benzyloxy series with the exception of **2** and especially **3** showing selective BuChE inhibition. From this series **3** showed the best multifunctional activity (eqBuChE IC<sub>50</sub> = 0.96 μM, hMAO-A IC<sub>50</sub> = 2.13 μM, hMAO-B IC<sub>50</sub> = 0.0021 μM). Within the *N*-benzylpiperidine (**16-19**) and *p*-bromo-*N*-benzylpiperazine (**21-24**) series the compounds in general showed moderate ChE and MAO-B inhibitory activity. Of these compounds **19** was the most potent multifunctional agent showing good eeAChE and eqBuChE inhibition (IC<sub>50</sub> = 9.10 μM and 5.90 μM, respectively), and relatively potent and selective hMAO-B inhibition (IC<sub>50</sub> = 0.30 μM, SI = >33). Molecular modeling revealed that **19** was able to bind simultaneously to the CAS, mid-gorge and PAS sites of AChE and BuChE suggesting that it will be able to inhibit AChE induced Aβ aggregation. From this study, compounds that **3** and **19** can be considered as promising multifunctional lead compounds.

**Keywords:** Alzheimer's disease, Coumarin, Donepezil, MAO-B, Cholinesterase, Molecular Modeling

---

## 1. Introduction

Alzheimer's disease (AD) is an age-related neurodegenerative disease characterised by progressive memory loss and decline in language skills, and other cognitive impairments [1]. Although the etiology of AD is not fully understood several factors, such as cholinergic dysfunction [2], τ-protein aggregation [3], amyloid-β (Aβ) deposits [4] and oxidative stress [5,6] are considered to play important roles in the pathophysiology of AD. The selective loss of cholinergic neurons in AD results in a deficit of acetylcholine (ACh) in specific regions of the brain that mediate learning and memory functions [7]. Consequently, AD patients have been treated with acetylcholinesterase (AChE) inhibitors [8-10] but unfortunately with limited therapeutic success, mainly because of the multifactorial nature of AD. Recent studies have also shown that compounds that are able to inhibit butyrylcholinesterase (BuChE) may be of value in the treatment of AD [11]. In AD the ratio of BuChE/AChE gradually increases as the disease progresses, partially as a consequence of the

progressive loss of the cholinergic synapses where AChE enzymes are located [12]. A compound able to inhibit both AChE and BuChE may thus be of more therapeutic value in AD. Alterations in other neurotransmitter systems, especially dopaminergic and serotonergic [13,14] are also thought to be responsible for the behavioral disturbances observed in AD [15]. This evidence has led to the suggestion that inhibitors of monoamine oxidase might also be of value in the treatment of AD [16,17].

Monoamine oxidase (MAO) is the enzyme that is responsible for the oxidative deamination of various biogenic and xenobiotic amines [18,19]. MAO exists as two isoforms, MAO-A and MAO-B, with MAO B being abundant in the brain [20]. The oxidative deamination catalysed by MAO-B leads to the production of neurotoxic products, such as hydrogen peroxide and aldehydes, which promote the formation of reactive oxygen species that cause oxidative stress and increased neuronal damage [21,22]. Studies have shown that the MAO-B activity in the brain of AD patients increases with time [23,24], thus increasing the rate of neuronal damage in the already diseased brain. MAO-A is more widely distributed peripherally than centrally, and as such, many side effects could occur if inhibited [25]. Therefore selective MAO-B inhibitors are better suited for the treatment of AD. Selegiline is a selective MAO-B inhibitor that has shown evidence of neuronal cell protection due to oxidative stress in AD patients [26], thereby confirming the important role of MAO-B in the cascade of events leading to neuronal cells death in AD.

The above observations has prompted the search for Multi-Target-Directed-Ligands (MTDLs), based on the “one molecule, multiple target” paradigm [27-29]. Thus, in this context, MTDLs able to simultaneously inhibit both cholinesterases and monoamine oxidases have been designed and investigated [30-39]. Among these MTDLs, Ladostigil has been approved for phase IIb clinical trials [31], which prompted us to search for new MTDLs with ChE and MAO-B inhibitory activity.

In this work we report the design, synthesis, biochemical evaluation and molecular modeling of coumarin structures conjugated with a benzyl-, piperidine-, *N*-benzylpiperidine- or *p*-bromo-*N*-benzylpiperazine moiety via a flexible alkyl ether linkage at the 7 coumarin position as MTDLs for the potential treatment of AD (Figure 1). Compounds were designed to incorporate coumarin structures known to show MAO-B inhibition [40] and selected structural elements of donepezil a selective AChE inhibitor currently used in the pharmacological treatment of AD [8]. Studies suggest that simultaneous inhibition of MAO-B and ChE does not only improve the level of ACh and reduce oxidative stress in the brain but also decreases A $\beta$  deposition which may make such a compound more effective against AD [34]. We expected that the coumarin moiety would be able to occupy the substrate cavity of MAO-B thereby conferring MAO-B inhibitory activity to the designed compounds. Substitutions were made on the 7-position of the coumarin moiety as previous studies showed that substitutions at this position lead to increased MAO-B activity and selectivity [40-43].

In addition to the above, the series of compounds were also designed to allow for exploration of the influence of various distinct functional group modifications on the 3- and/or 4-position of the coumarin structure. In order to maximize ChE activity, the coumarin and the *N*-benzylpiperidine derivatives/portions were connected by a flexible alkyl chain. This linkage is expected to allow the *N*-benzylpiperidine derivative to interact with the catalytic anionic site (CAS), in a similar manner as donepezil, and the coumarin moiety to reach and interact with the peripheral anionic site (PAS) of AChE. Targeting both the CAS and PAS should result in significant AChE inhibitory activity while possibly inhibiting the  $A\beta$  pro-aggregating action of AChE via the PAS interaction [44-47]. All designed compounds (**1-25**) were synthesized and evaluated for their ability to inhibit ChEs and MAOs. The data of the structurally related compounds **26-29**, recently reported by Sai-Sai *et al.*, 2016 [39], were included in this report in order to compare certain structural elements with compounds **1-25** and draw up a comprehensive list of structure activity relationships.

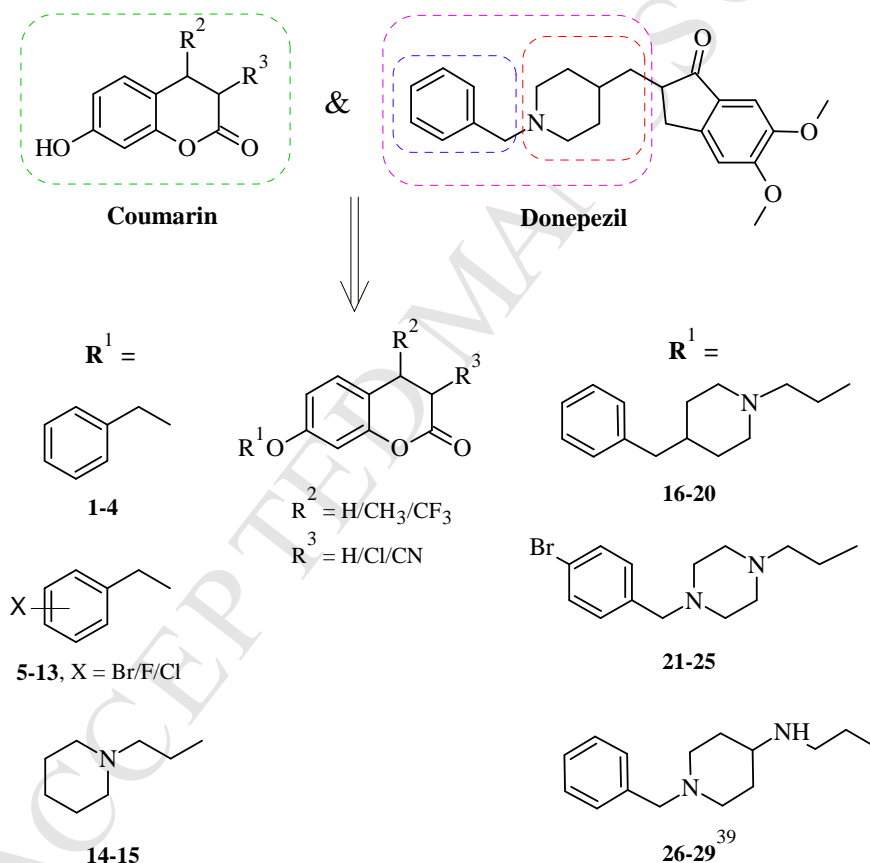


**Figure 1:** Design strategy for the 7-substituted coumarins incorporating different portions and distinct variations of the *N*-benzylpiperidine moiety of donepezil.

## 2. Results and discussion

### 2.1. Chemistry

Compound **1-15** were synthesised (Figure 2) by conjugating the commercially available 7-hydroxycoumarin derivatives (**1a-5a**) to a benzylbromide- (**1-4**), halogen substituted benzylbromide- (**5-13**) or 1-(2-chloroethyl)piperidine (**14** and **15**) moiety through an  $S_N2$  nucleophilic substitution reaction using ethanol (**1-13**) or acetonitrile (**14** and **15**) as solvent in the

presence of potassium carbonate. The synthesis of compounds **16-25** (Figure 3) commenced from coumarins **1-5a** which were conjugated with an excess of a 1,2-dibromoethane linker to afford the key intermediates **1b-5b**. These intermediates were then treated with *N*-benzylpiperidine or 1-(4-bromobenzyl)piperazine in the presence of potassium carbonate in acetonitrile to give the target compounds **16-25**.

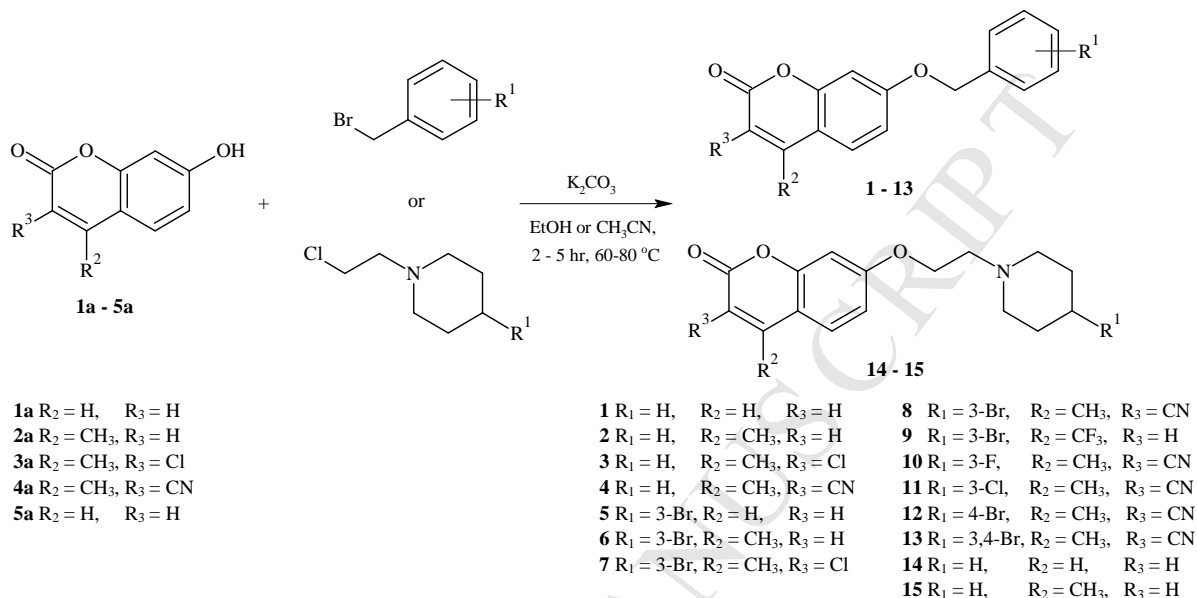


**Figure 2:** Synthetic pathway for the synthesis of compounds **1-15**.

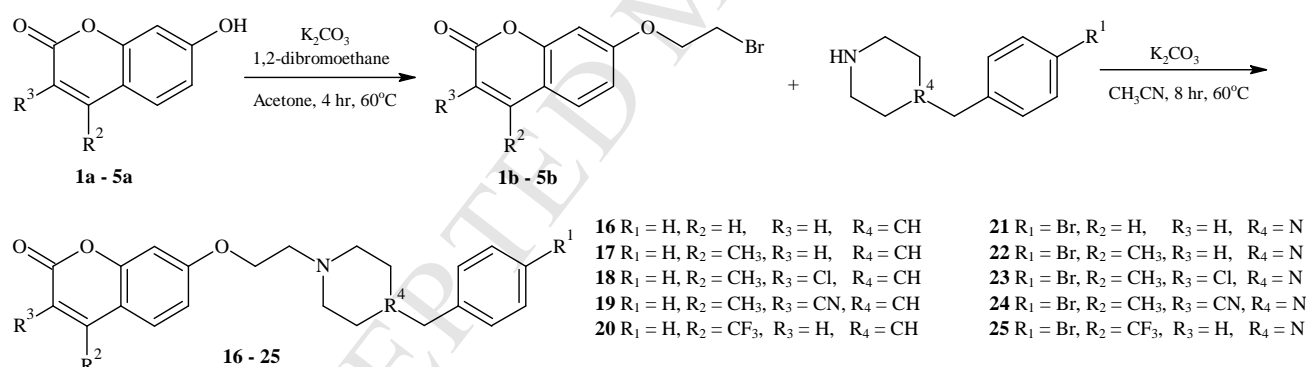


**Figure 3:** Synthetic pathway for the synthesis of compounds **16-25**.

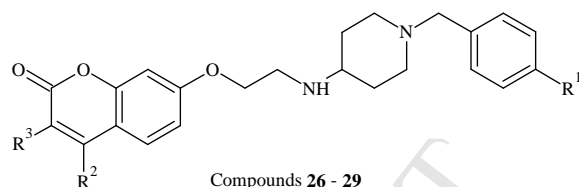
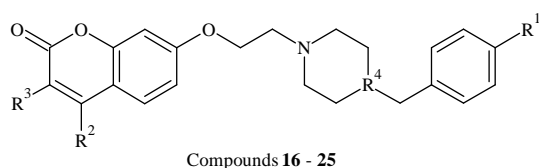
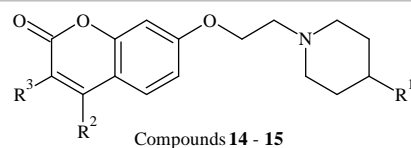
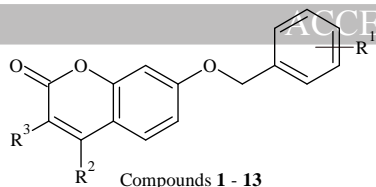
## 2.2. Monoamine oxidase inhibition studies

The target compounds (**1-25**) were investigated for their inhibitory activity against hMAO by measuring the extent by which the test inhibitor reduces the MAO-catalysed oxidation of kynuramine, a mixed MAO-A/B substrate [48,49]. The inhibition potencies of the test inhibitors (**1-25**, **26-29** [39]) and reference compounds, selegiline and clorgyline, were expressed as IC<sub>50</sub> values and are presented in Table 1. The results indicate that all the test compounds have better inhibitory activity for MAO-B over MAO-A with SI values ranging from >2 – 1310. This corresponds well to previous studies where it was found that coumarin structures substituted at the 7-position with various distinct functional moieties show selective MAO-B inhibition [40-43].

Compounds **1-8** showed highly potent activity ( $IC_{50}$ : 0.5–3.8 nM) that was better than the positive control selegiline ( $IC_{50} = 8$  nM). The bromobenzyl-coumarin moieties (**5-8**) in general have slightly better inhibitory activity for MAO than the benzyl-coumarin moieties (**1-4**). This corresponds to the observations made by Gnerre *et al* [41] wherein they noted that an increase in activity toward MAO is seen when a halogen is substituted on the para-position of the benzyl ring. The same para-bromine substitution however decreased the degree of MAO-B selectivity of the compounds (Table 1). Other halogen substitutions on the para and/or meta position(s) on the benzyl ring (**10-13**) did not improve the inhibitory activity of compounds **4** and **8** indicating that the bulk of the para-bromine substitution is favoured. Replacing the benzyl- with an ethylpiperidine moiety (**14-15**) lead to a drastic decrease in MAO-B activity, signifying the importance of the aromatic benzyl function. The substituents at the 3- and/or 4-position of the coumarin moiety did not, in general, influence the activities on MAOs with the exception of compound **9** where the  $CF_3$  substitution at the 4 position lead to a significant decrease in activity. This could indicate that electron withdrawing hydrophobic substitutions on position 4 is not tolerated in the active site cavity of MAOs.

The addition of the piperidine (**16-20** and **26-29** [39]) or piperazine (**21-25**) function between the benzyl and coumarin moieties lead to a decrease in MAO activity compared to compounds **1-13** (Table 1). This decrease in activity could be attributed to the larger substitutions on position 7 of the coumarin moiety as suggested by Brühlmann *et al.*, 2001 [30]. The compounds, as expected, did not show any activity towards MAO-A, but did show promising activity towards MAO B inhibition ( $IC_{50}$ : 0.29-5.64  $\mu$ M). Unlike what was observed with compounds **5-8**, the para-bromine substitution on the benzyl moiety (**21-25**) reduced the inhibitory capacity of these compounds. A reason for the decrease in activity observed could be the presence of the piperazine moiety instead of the piperidine moiety. When the piperidine-containing compounds **16-20** are compared to the piperidine-containing compounds (**26-29** [39]), it is noticeable that the position of the nitrogen in the piperidine moiety influences the MAO-B activity. When the piperidine nitrogen is connected to the coumarin (**16-20**) a 5–50 fold increase in MAO-B activity is observed compared to when the piperidine nitrogen is connected to the benzyl moiety (**26-29**). The linker, containing an additional amine function, between the coumarin and piperidine moiety may also have influenced the activity of these compounds. When compounds **16-17** are compared to their counterparts lacking the benzyl moiety (**14-15**) a definite increase in activity is observed signifying the importance of the benzyl moiety in these structures. As observed with compounds **1-13**, substituents at the 3- and/or 4-position did not, in general, influence the MAO-B activities.

**Table 1:** *In vitro*  $IC_{50}$  values of test compounds **1-15** for hMAO-A, hMAO-B, eeAChE and eqBuChE.



Compound	R <sub>1</sub>	R <sub>2</sub>	R <sub>3</sub>	R <sub>4</sub>	MAO-A IC <sub>50</sub> μM	MAO-B IC <sub>50</sub> μM	SI MAO-B <sup>a</sup>	AChE IC <sub>50</sub> μM	BuChE IC <sub>50</sub> μM	SI AChE <sup>b</sup>
<b>1</b>	H	H	H	-	3.49	0.0038	930	>100	>100	-
<b>2</b>	H	CH <sub>3</sub>	H	-	2.62	0.0020	1310	>100	9.60	<0.10
<b>3</b>	H	CH <sub>3</sub>	Cl	-	2.13	0.0021	1024	>100	0.96	<0.01
<b>4</b>	H	CH <sub>3</sub>	CN	-	1.38	0.0019	700	>100	21.80	<0.22
<b>5</b>	<i>p</i> -Br	H	H	-	0.24	0.0005	480	>100	>100	-
<b>6</b>	<i>p</i> -Br	CH <sub>3</sub>	H	-	0.05	0.0009	56	>100	>100	-
<b>7</b>	<i>p</i> -Br	CH <sub>3</sub>	Cl	-	0.37	0.0008	463	>100	>100	-
<b>8</b>	<i>p</i> -Br	CH <sub>3</sub>	CN	-	0.05	0.0013	38	>100	>100	-
<b>9</b>	<i>p</i> -Br	CF <sub>3</sub>	H	-	>10	0.104	>96	>100	>100	-
<b>10</b>	<i>p</i> -F	CH <sub>3</sub>	CN	-	0.60	0.0022	273	>100	>100	-
<b>11</b>	<i>p</i> -Cl	CH <sub>3</sub>	CN	-	1.13	0.013	87	>100	>100	-
<b>12</b>	<i>o</i> -Br	CH <sub>3</sub>	CN	-	>10	0.073	>137	>100	>100	-
<b>13</b>	<i>o, p</i> -Br	CH <sub>3</sub>	CN	-	0.72	0.018	40	>100	>100	-
<b>14</b>	H	H	H	-	n.d.	9.21	-	54.90	n.d.	-
<b>15</b>	H	CH <sub>3</sub>	H	-	n.d.	3.09	-	66.43	n.d.	-
<b>16</b>	H	H	H	CH	>10	0.47	>21	36.70	20.30	0.47
<b>17</b>	H	CH <sub>3</sub>	H	CH	>10	0.53	>19	29.40	5.19	0.18
<b>18</b>	H	CH <sub>3</sub>	Cl	CH	>10	0.29	>34	31.30	1.27	0.04
<b>19</b>	H	CH <sub>3</sub>	CN	CH	>10	0.30	>33	9.10	5.90	0.67
<b>20</b>	H	CF <sub>3</sub>	H	CH	>10	5.33	>2	>100	>100	-
<b>21</b>	Br	H	H	N	>10	1.70	>6	>100	50.10	0.53
<b>22</b>	Br	CH <sub>3</sub>	H	N	>10	3.60	>3	12.8	9.70	0.76
<b>23</b>	Br	CH <sub>3</sub>	Cl	N	>10	1.55	>7	>100	3.12	<0.03
<b>24</b>	Br	CH <sub>3</sub>	CN	N	>10	1.41	>7	38.5	13.30	0.35
<b>25</b>	Br	CF <sub>3</sub>	H	N	>10	5.64	>2	>100	>100	-
<b>26<sup>c</sup></b>	H	H	H	-	>100	8.39	>12	4.42	5.34	1.21
<b>27<sup>c</sup></b>	H	CH <sub>3</sub>	H	-	>100	2.75	>36	5.62	4.38	0.78
<b>28<sup>c</sup></b>	H	CH <sub>3</sub>	Cl	-	>100	14.7	>7	1.58	1.42	0.90
<b>29<sup>c</sup></b>	H	CF <sub>3</sub>	H	-	>100	28.5	>4	9.18	10.22	1.11
<b>Selegiline</b>	-	-	-	-	n.d.	0.008	-	n.d.	n.d.	-
<b>Clorgyline</b>	-	-	-	-	0.001	n.d.	-	n.d.	n.d.	-
<b>Donepezil</b>	-	-	-	-	n.d.	n.d.	-	0.007	2.87	428
<b>Tacrine</b>	-	-	-	-	n.d.	n.d.	-	0.102	0.017	0.17

<sup>a</sup>hMAO-B selectivity index = IC<sub>50</sub>(hMAO-A)/IC<sub>50</sub>(hMAO-B). <sup>b</sup>AChE selectivity index = IC<sub>50</sub>(eqBuChE)/IC<sub>50</sub>(eeAChE).

<sup>c</sup>Data taken from Sai-Sai *et al* [39]. n.d. = not determined.

The inhibitory activity of the target compounds **1-25** against eeAChE (from electric eel) and eqBuChE (from equine serum) were measured according to the method of Ellman *et al.*, using tacrine and donepezil as reference compounds [50,51]. The IC<sub>50</sub> values of the test compounds and reference compounds are given in Table 1 (**1-25**, **26-29** [39]). Compounds **1**, **5-13** showed little to no inhibitory activity towards either of the cholinesterases at a 100 μM concentration. These results were as expected because these compounds lack the *N*-benzylpiperidine or similar moiety of donepezil. However, an unexpected result was observed for compounds **2-4** were selective and moderately potent BuChE inhibitory activity, especially for compound **3** (IC<sub>50</sub> = 0.96 μM, SI > 104) was observed. The addition of the para-bromine moiety to the benzyl function (**6-8**) abolished the cholinesterase inhibitory activity of these compounds (**2-4**). In contrast to what was observed in the MAO studies the substituents at the 3- and/or 4-position of the coumarin moiety did influence the ChE activities of **1-5**. The addition of a methyl at position 4 (**2**) increased the BuChE inhibitory activity (IC<sub>50</sub> = 9.60 μM) compared to compound **1** (IC<sub>50</sub> > 100 μM). Adding a chlorine on position 3 while retaining the methyl at position 4 (**3**) increased the BuChE activity and selectivity even further as seen by the IC<sub>50</sub> values. Replacing the chlorine with a nitrile (**4**) decreased the activity (IC<sub>50</sub> = 21.80 μM) and a CF<sub>3</sub> substitution at position 4 (**5**) rendered the compound inactive.

Compounds (**16-19**) containing the *N*-benzylpiperidine moiety showed moderate inhibitory activity against both ChEs with some slight selectivity towards BuChE. When these compounds are compared to their reported counterparts (**26-29**) [39] it is evident that they show similar BuChE activity, however the AChE activity for **16-19** decreased. The substituents at the 3- and/or 4-position did not influence the ChE activities of **26-29** as previously reported [39], but did influence the ChE activity of **16-20**. Especially compound **19** with a methyl substituent at the 4 position and a nitrile substituent at the 3 position showed a marked improvement in AChE activity. This implies that compounds **16-20** can be further explored to improve their AChE activity based on distinct substitutions on the 3- and/or 4-position without affecting MAO-B activity. Sugimoto *et al.*, 2000 [52] demonstrated that replacement of the piperidine with a piperazine moiety, as is the case with compounds **20-25**, drastically decreases AChE activity of donepezil. This same effect, although not as pronounced as in Sugimoto's study, was observed with compounds **21-25**.

#### 2.4. Molecular modeling

The enzyme assays point to **3** and **19** as promising multitarget inhibitors. To provide insight, the binding mode of **3** and **19** in hMAO-A, hMAO-B, eeAChE and eqBuChE were examined using molecular docking. The structures of human MAO-A co-crystallized with harmine (PDB entry: 2Z5X) [53], human MAO-B co-crystallized with 7-(3-chlorobenzyloxy)-4-(methylamino)methyl-

coumarin (PDB entry: 2V61) [43] and eeAChE co-crystallized with donepezil (PDB entry: 1EVE) [54] were retrieved from the Brookhaven Protein Data Bank ([www.rcsb.org/pdb](http://www.rcsb.org/pdb)) and the docking was carried out with the Dock application of the Molecular Operating Environment (MOE) software [55]. With respect to BuChE, in the absence of a X-ray structure of eqBuChE, a homology model was used to rationalize the experimental data. The modeling of the 3D structure was performed by an automated homology-modeling program (SWISS-MODEL) [56-57]. This putative three-dimensional structure of eqBuChE has been created based on the crystal structure of hBuChE (PDB: 2PM8) as these two enzymes exhibited 89% sequence identity. The docking of the compounds into this homology model of eqBuChE was carried out with Autodock Vina software [58] using a grid box that was placed over the active site. The docking results generated were directly loaded into and analyzed with MOE.

#### 2.4.1. MAO molecular modeling studies

The MAO inhibition studies show that all the test compounds (**1-25**) showed selective MAO-B activity over MAO-A. To provide additional insight into the selective MAO-B inhibitory activity, the binding modes of compound **3** and **19** in MAO-A and MAO-B were examined using molecular docking. The best-ranked docking solutions of compounds **3** and **19** within the active site of MAO-B shows that the coumarin moiety of both compounds bind in the polar region of the substrate cavity in the vicinity of the FAD co-factor and the 'aromatic sandwich' defined by Tyr398 and Tyr435 (Figure 4). The binding orientation of the coumarin moiety of **3** and **19** are similar to that observed for the co-crystallized coumarin within the active site of MAO-B [43]. The carbonyl moiety of **3** showed a hydrogen bond interaction with Cys172 similar to the co-crystallized coumarin. Docking simulations of compounds **1-2** and **4-8** also showed this hydrogen bond interaction with Cys172 (data not shown). The nitrile on the 3 position of **19** exhibited a hydrogen bond interaction with N5 of FAD but was lacking the interaction with Cys172. As indicated by the biological results the substitutions at the 3- and/or 4 position did not largely influence the MAO-B activity of compounds **1-8** and **16-19**. Therefore the interaction of the nitrile of **19** with FAD seems to be less important than the interaction with Cys172. This may explain why **19** had lower MAO-B activity compared to **3**. The benzyl- and *N*-benzylpiperidine side chain of **3** and **19** extends past Ile199 which is situated in the entrance cavity of the enzyme. Within the hydrophobic environment of the entrance cavity, the benzyl- and *N*-benzylpiperidine side chain is most likely stabilized by Van der Waals interactions. These favorable binding orientations and interactions of **3** and **19** may explain the potent and moderate MAO-B activity, respectively, observed for these compounds. The docking results of **3** and **19** in complex with MAO-A (data not shown) showed that in both cases the coumarin moiety was stabilized in the entrance cavity compared to the substrate cavity as observed

for these compounds in MAO-B. This observation may explain the selective MAO-B activity of the test compounds.

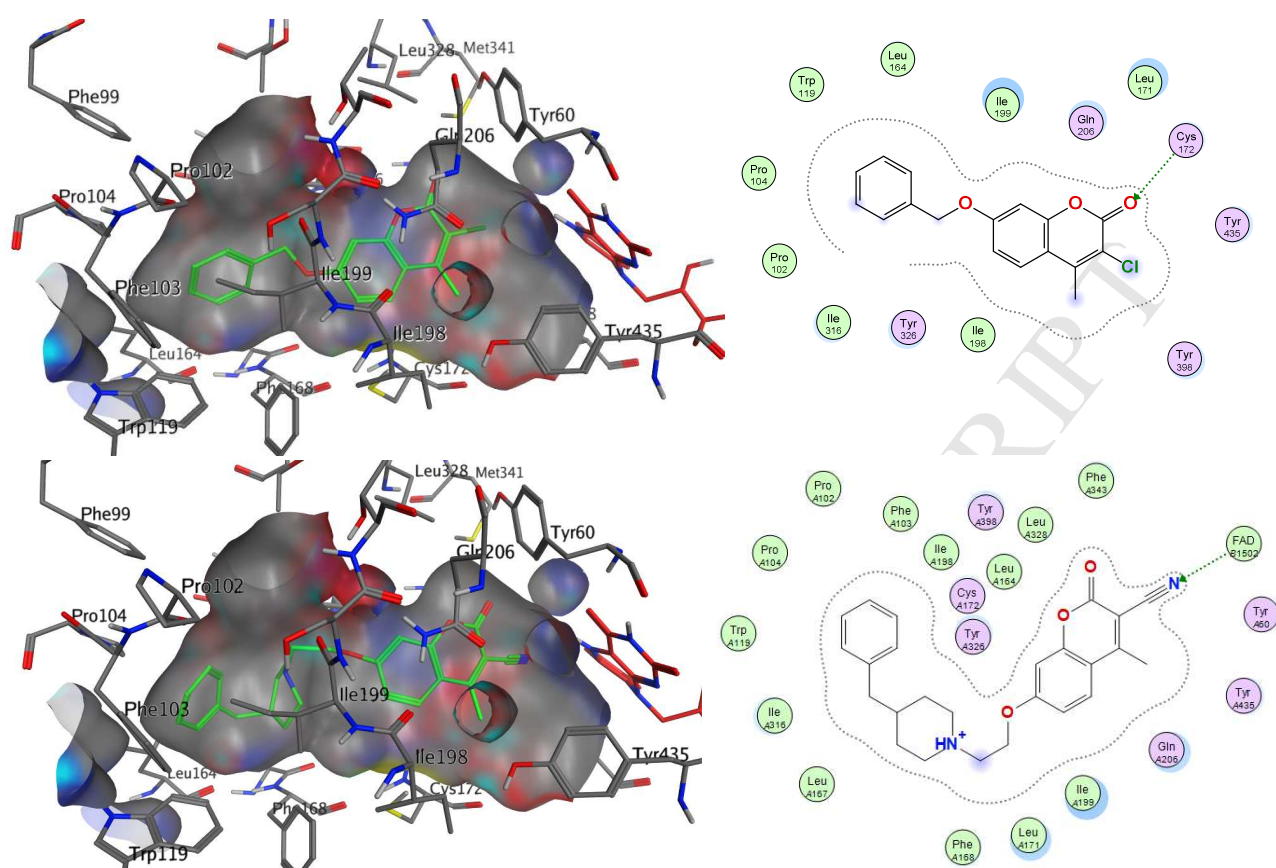


**Figure 4:** The hMAO-B active site cavity (left) and interaction maps (right) displaying the binding and interactions of compounds **3** (top) and **19** (bottom). FAD is shown in red and the compounds are shown in green in the active site cavity.

#### 2.4.2. Cholinesterase molecular modeling studies

As indicated by the biological results, compound **3** showed selective BuChE inhibitory activity over AChE and compound **19** presented with both AChE and BuChE inhibitory activity. Molecular docking was thus employed to gain some insight into the binding modes of these compounds. The docking results of compounds **3** and **19** docked within the active site of eeAChE are shown in Figure 5. Compound **3** binds to AChE with its coumarin moiety sitting in the area of the PAS and its benzyl moiety reaching the mid-gorge [54,59]. No interactions with any of the surrounding residues were predicted by the software. Therefore the inability of **3** to reach the CAS and no interactions with surrounding residues may explain the lack of AChE inhibitory activity. The docking results of **19** showed that the coumarin moiety binds to the PAS site of the enzyme, establishing a  $\pi$ - $\pi$  stacking interaction between its phenyl ring and the indole ring of Trp279. The piperidine moiety of **19** interacts with Tyr324 in the mid-gorge and similar to donepezil, the *N*-benzylpiperidine moiety is located at the CAS, which showed a  $\pi$ - $\pi$  stacking interaction with Trp84 [54,59]. The ability of **19** to

interact with both the CAS and PAS sites of AChE could explain the inhibitory activity observed and indicate that **19** could have the ability to inhibit the A $\beta$  pro-aggregating action of AChE [44-47].

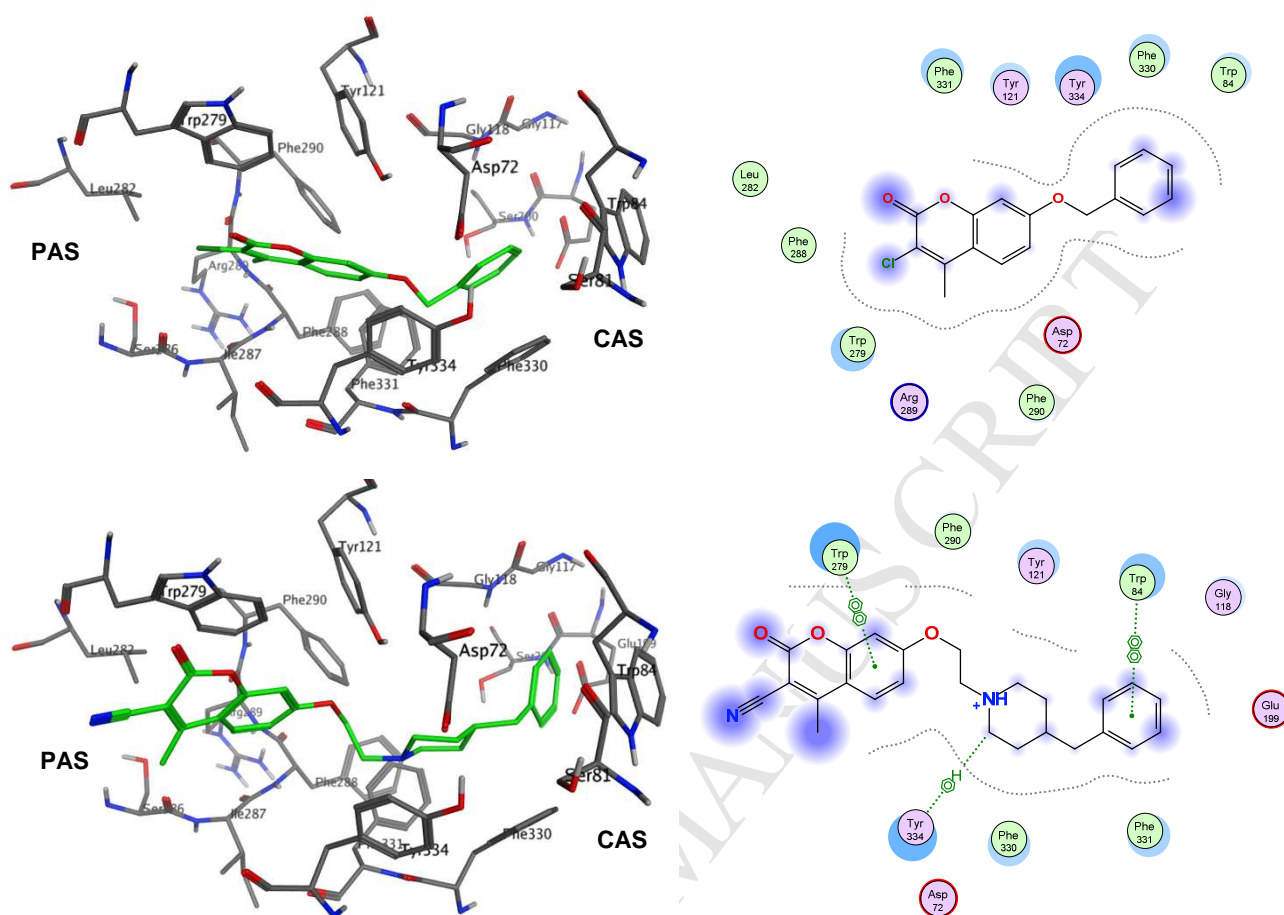


**Figure 5:** The eeAChE active site cavity (left) and interaction map (right) displaying the binding and interactions of compounds of **3** (top) and **19** (bottom).

The binding mode of **3** and **19** at the active site of the eqBuChE homology build model is illustrated in Figure 6. The docking results of **3** showed that the benzyl- and coumarin moieties bind in the CAS and PAS region of the enzyme respectively [59], establishing  $\pi$ - $\pi$  stacking interactions with Trp82 and Tyr332. This favourable position of **3** within the active site of eqBuChE may account for the higher affinity and selectivity observed for BuChE over AChE. As depicted in Figure 7, **19** was well accommodated inside the active site gorge and showed a binding mode with a U-shaped conformation. The lowest energy binding orientation of **19** enabled the benzyl moiety to interact with Trp82 in the CAS allowing a  $\pi$ - $\pi$  stacking interaction. A hydrogen bond between the piperidine  $\text{NH}^+$  and Asp70 is observed in the PAS region of the enzyme. The carbonyl of the coumarin moiety interacted though a hydrogen bond with the catalytic-triad residue Ser198 [59]. These important interactions of **3** and **19** may explain the good BuChE activities observed for these compounds.

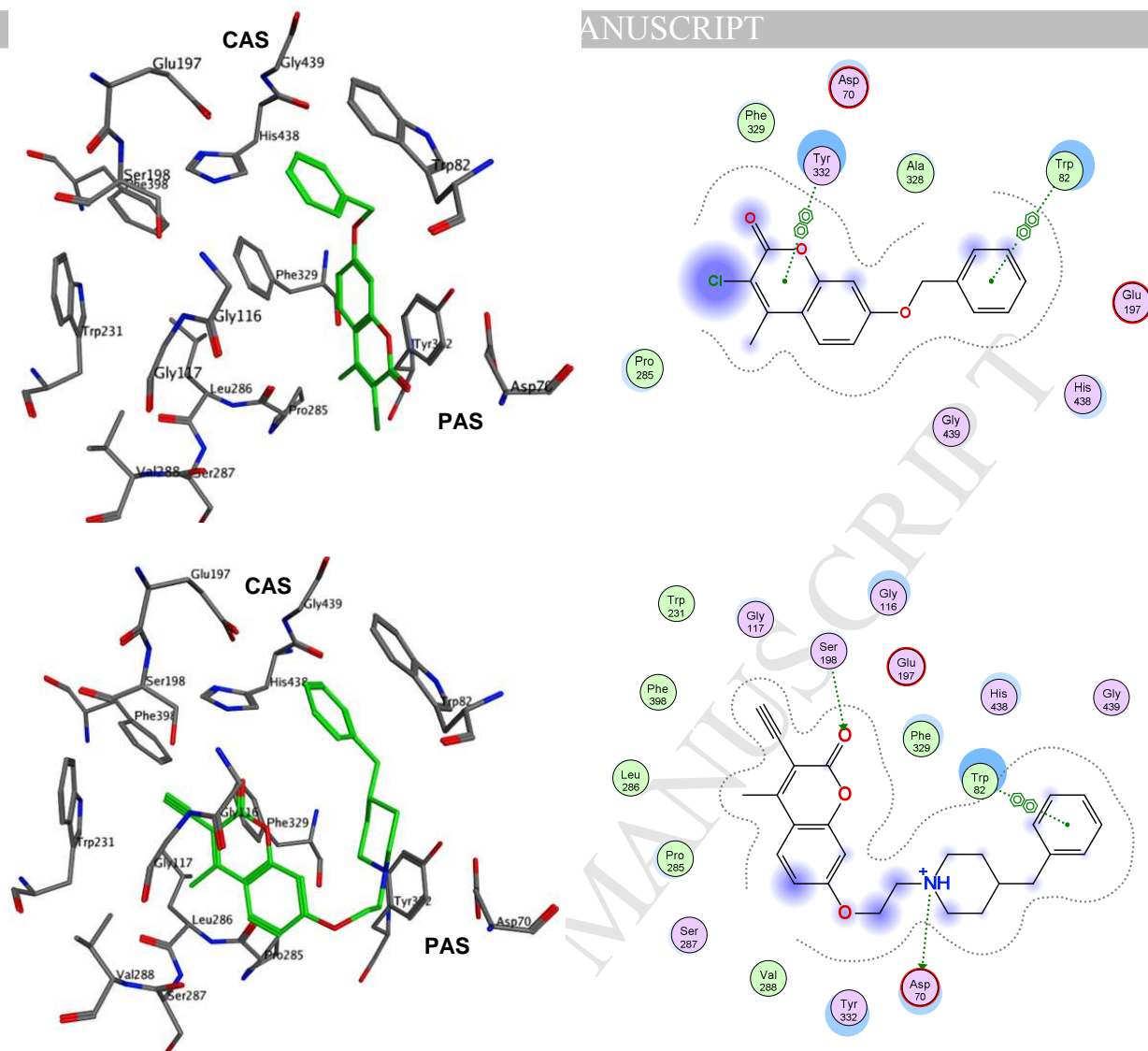


**Figure 6:** Complex of compound **3** (top) and **19** (bottom) with the eqBuChE homology model (left) and the interaction maps (right).

### 3. Conclusion

A series of 7-substituted coumarin derivatives was designed and synthesized as multipotent inhibitors able to selectively inhibit hMAO-B, as well as eeAChE and eqBuChE. Compound **3** can be considered as a new multifunctional lead compound because of its potent MAO-B ( $IC_{50} = 0.0021 \mu M$ ) and moderate BuChE ( $IC_{50} = 0.96 \mu M$ ) inhibitory activities. Molecular modeling revealed the favourable binding modes and important interactions of **3** in the active sites of BuChE and MAO-B. Considering the increasing attention given to BuChE [11,60,61] and the ability of **3** to inhibit MAOs, this compound might be advantageous in AD treatment and should be investigated further. Compound **19** was also identified as a MTDL being able to selectively inhibit hMAO-B ( $IC_{50} = 0.30 \mu M$ , SI >33) and inhibit both eeAChE ( $IC_{50} = 9.10 \mu M$ ) and eqBuChE ( $IC_{50} = 5.90 \mu M$ ). Docking studies indicated that the promising hMAO-B inhibitory activity of **19** may be ascribed to the position of the coumarin in the substrate cavity and the ability of the benzyl moiety to occupy the

entrance cavity. Further *in silico* studies showed that **19** is able to bind to both the CAS and PAS of AChE and BuChE. Based on the role played by PAS in the induction of A $\beta$  aggregation by AChE it is expected that **19** would show inhibition of hAChE induced A $\beta$  aggregation. This study has thus provided new insights into the structure activity relationships of these compounds and could possibly afford new attractive and more promising drugs for the treatment of AD.

## 4. Experimental section

### 4.1. Chemistry

Unless otherwise specified, materials were obtained from commercial suppliers and used without further purification. All reactions were monitored by thin-layer chromatography on 0.20 mm thick aluminium silica gel sheets (Alugram<sup>®</sup> SIL G/UV<sub>254</sub>, Kieselgel 60, Macherey-Nagel, Düren, Germany). Visualisation was achieved using UV light (254 nm and 366 nm), an ethanol solution of ninhydrin or iodine vapours, with mobile phases prepared on a volume-to-volume basis. Chromatographic purifications were performed on silica gel (0.063–0.2 mm, Sigma Aldrich) except when otherwise stated. The MS spectra were recorded on a Perkin Elmer Flexar SQ 300 mass spectrometer by means of direct injection with a syringe pump. High resolution electron spray ionisation (HREI) mass spectra for all compounds were recorded on a Waters API Q-ToF Ultima mass spectrometer at 70 eV and 100 °C. The IR spectra were recorded on a Perkin Elmer Spectrum 400 spectrometer, fitted with a diamond attenuated total reflectance (ATR) attachment. Melting points were determined using a Stuart SMP-300 melting point apparatus and capillary tubes. All the melting points determined were recorded uncorrected. <sup>1</sup>H and <sup>13</sup>C NMR spectra were determined using a Bruker Avance III HD spectrometer at a frequency of 400 MHz and 100 MHz, respectively. Tetramethylsilane (TMS) was used as internal standard. All chemical shifts are reported in parts per million (ppm), relative to the internal standard. The following abbreviations are used to indicate the multiplicities of the respective signals: s - singlet; s - broad singlet; d - doublet; dd - doublet of doublets; t - triplet and m - multiplet.

### 4.2. General procedure for the synthesis of compounds 1-13

The appropriate commercially available 7-hydroxycoumarin (1 mmol, **1a–5a**) and K<sub>2</sub>CO<sub>3</sub> (1.1 mmol) were dissolved in 10 ml ethanol. To the mixture, benzylbromide (1 mmol for compounds **1–4**) or the appropriate bromobenzyl derivative (1 mmol for compounds **5–13**) was added depending on the compound to be synthesised. The mixture was stirred under reflux conditions until the reaction reached completion (monitored by TLC, mobile phase = EtOAc). Once the reaction was complete, 20 ml of distilled water was added and the mixture was allowed to cool to room temperature. This resulted in the formation of a precipitate that was filtered off and allowed to dry

overnight in a fume cupboard rendering the pure 7-(benzyloxy)coumarin derivatives (**1–13**) as off-white amorphous solids.

#### 4.2.1. 7-(Benzyloxy)-2*H*-chromen-2-one (**1**)

Yield: 56 % mp: 155 °C; <sup>1</sup>H NMR: (400 MHz, CDCl<sub>3</sub>) δ<sub>H</sub>: 7.64–7.60 (d, 1H, J = 9.2 Hz), 7.42–7.35 (m, 5H), 6.92–6.87 (m, 2H), 6.26–6.22 (d, 1H, J = 9.2 Hz), 5.11 (s, 2 H); <sup>13</sup>C NMR (100 MHz, CDCl<sub>3</sub>): 161.84, 161.13, 155.78, 143.33, 135.72, 128.72, 128.35, 127.47, 113.21, 112.69, 101.88, 70.48; IR (ATR, cm<sup>-1</sup>): 1707, 1110, 693; MS (EI, 70 eV) m/z: 253.10 [M+H]<sup>+</sup>; HR-ESI [M+H]<sup>+</sup>: calcd. 259.0859, found. 259.0862.

#### 4.2.2. 7-(Benzyloxy)-4-methyl-2*H*-chromen-2-one (**2**)

Yield: 52 % mp: 130 °C; <sup>1</sup>H NMR: (400 MHz, CDCl<sub>3</sub>) δ<sub>H</sub>: 7.49–7.41 (d, 1H, J = 8.8 Hz), 7.42–7.33 (m, 5H), 6.94–6.90 (d, 1H, J = 8.8 Hz), 6.88 (s, 1H), 6.12 (s, 1H), 5.12 (s, 2H), 2.38 (s, 3H); <sup>13</sup>C NMR (100 MHz, CDCl<sub>3</sub>): 161.71, 161.29, 155.23, 152.53, 135.85, 128.77, 128.38, 127.53, 125.58, 113.80, 112.95, 112.09, 101.96, 70.49, 18.68; IR (ATR, cm<sup>-1</sup>): 3032, 1706, 699; MS (EI, 70 eV) m/z: 267.14 [M+H]<sup>+</sup>; HR-ESI [M+H]<sup>+</sup>: calcd. 267.1016, found. 267.1018.

#### 4.2.3. 7-(Benzyloxy)-3-chloro-4-methyl-2*H*-chromen-2-one (**3**)

Yield: 49 % mp: 145–146 °C; <sup>1</sup>H NMR: (400 MHz, CDCl<sub>3</sub>) δ<sub>H</sub>: 7.53–7.50 (d, 1H, J = 8.8 Hz), 7.41–7.34 (m, 5 H), 6.98–6.95 (d, 1H, J = 8.8 Hz), 6.88 (s, 1H), 5.12 (s, 2H), 2.53 (s, 3H); <sup>13</sup>C NMR (100 MHz, CDCl<sub>3</sub>): 161.52, 157.34, 152.98, 147.84, 135.57, 128.71, 128.37, 127.44, 125.83, 117.85, 113.55, 113.41, 101.78, 70.51, 16.08; IR (ATR, cm<sup>-1</sup>): 3057, 1707, 750, 696; MS (EI, 70 eV) m/z: 301.05 [M+H]<sup>+</sup>; HR-ESI [M+H]<sup>+</sup>: calcd. 301.0626, found. 301.0621.

#### 4.2.4. 7-(Benzyloxy)-4-methyl-2-oxo-2*H*-chromene-3-carbonitrile (**4**)

Yield: 12 % mp: 136 °C; <sup>1</sup>H NMR: (400 MHz, CDCl<sub>3</sub>) δ<sub>H</sub>: 7.64–7.61 (d, 1H, J = 8.8 Hz), 7.41–7.37 (m, 5H), 7.03–7.00 (d, 1H, J = 8.8 Hz), 6.89 (s, 1H), 5.16 (s, 2H), 2.70 (s, 3H); <sup>13</sup>C NMR (100 MHz, CDCl<sub>3</sub>): 164.43, 162.06, 157.33, 155.54, 135.06, 128.85, 128.68, 127.56, 127.31, 114.63, 113.90, 112.10, 102.11, 98.84, 70.93, 18.14; IR (ATR, cm<sup>-1</sup>): 3079, 1722, 1611, 682; MS (EI, 70 eV) m/z: 292.14 [M+H]<sup>+</sup>; HR-ESI [M+H]<sup>+</sup>: calcd. 292.0968, found. 292.0976.

#### 4.2.5. 7-[(4-Bromobenzyl)oxy]-2*H*-chromen-2-one (**5**)

Yield: 68%; mp: 160 °C; <sup>1</sup>H NMR: (400 MHz, CDCl<sub>3</sub>) δ<sub>H</sub>: 7.65 – 7.61 (d, 1H, J = 9.6 Hz), 7.60 – 7.50 (d, 2H, J = 8.4 Hz), 7.40–7.35 (d, 1H, J = 8.4 Hz), 7.32 – 7.28 (d, 2H, J = 8.4 Hz), 6.95–6.88 (dd, 1H, J = 8.8, 2.4 Hz), 6.87–6.84 (m, 1H), 6.28–6.24 (d, 1H, J = 9.6 Hz), 5.11 (s, 2H); <sup>13</sup>C NMR (100 MHz, CDCl<sub>3</sub>): 161.51, 161.04, 155.77, 143.28, 134.75, 131.89, 129.09, 128.84, 122.34, 113.39, 113.13, 112.86, 101.87, 69.69; IR (ATR, cm<sup>-1</sup>): 3068, 2257, 1705, 1128, 686; MS (EI, 70 eV) m/z: 330.93 [M+H]<sup>+</sup>; HR-ESI [M+H]<sup>+</sup>: calcd. 330.9964, found. 330.9959.

#### 4.2.6. 7-[(4-Bromobenzyl)oxy]-4-methyl-2H-chromen-2-one (6)

Yield: 68%; mp: 153 °C;  $^1\text{H NMR}$ : (400 MHz,  $\text{CDCl}_3$ )  $\delta_{\text{H}}$ : 7.54–7.49 (m, 3H), 7.32–7.29 (d, 2 H,  $J = 8.4$  Hz), 6.93–6.88 (dd, 1H,  $J = 8.8, 2.4$  Hz), 6.87–6.85 (m, 1H), 6.14 (s, 1H), 5.07 (s, 2H), 2.39 (s, 3H);  $^{13}\text{C NMR}$ : (100 MHz,  $\text{CDCl}_3$ ): 161.35, 161.19, 155.18, 152.46, 134.84, 131.90, 129.12, 125.63, 122.34, 113.95, 112.85, 112.23, 101.91, 69.67, 18.68; **IR** (ATR,  $\text{cm}^{-1}$ ): 3074, 1707, 1070, 680; **MS** (EI, 70 eV)  $m/z$ : 344.94  $[\text{M}+\text{H}]^+$ ; **HR-ESI**  $[\text{M}+\text{H}]^+$ : calcd. 345.0121, found. 345.0118.

#### 4.2.7. 7-[(4-Bromobenzyl)oxy]-3-chloro-4-methyl-2H-chromen-2-one (7)

Yield: 61 %; mp: 191 – 192 °C;  $^1\text{H NMR}$ : (400 MHz,  $\text{CDCl}_3$ )  $\delta_{\text{H}}$ : 7.55–7.51(m, 3H), 7.32–7.28 (d, 2 H,  $J = 8.4$  Hz), 6.98–6.95 (dd, 1 H,  $J = 8.8, 2.4$  Hz), 6.88–6.85 (m, 1H), 5.08 (s, 2 H), 2.26 (s, 3 H);  $^{13}\text{C NMR}$  (100 MHz,  $\text{CDCl}_3$ ): 161.26, 157.36, 153.04, 147.87, 134.67, 131.96, 129.15, 126.01, 122.45, 118.12, 113.68, 113.55, 101.85, 69.79, 16.20; **IR** (ATR,  $\text{cm}^{-1}$ ): 3074, 1725, 1600, 801, 683; **MS** (EI, 70 eV)  $m/z$ : 379.18  $[\text{M}+\text{H}]^+$ ; **HR-ESI**  $[\text{M}+\text{H}]^+$ : calcd. 378.9131, found. 378.9136.

#### 4.2.8. 7-[(4-Bromobenzyl)oxy]-4-methyl-2-oxo-2H-chromene-3-carbonitrile (8)

Yield: 55%; mp: 186 – 187 °C;  $^1\text{H NMR}$ : (400 MHz,  $\text{CDCl}_3$ )  $\delta_{\text{H}}$ : 7.66–7.63 (d, 1H,  $J = 9.2$  Hz), 7.56–7.53 (d, 2H,  $J = 8.0$  Hz), 7.32–7.28 (d, 2H,  $J = 8.0$  Hz), 7.03–6.99 (dd, 1H,  $J = 8.8, 2.4$  Hz), 6.88 (s, 1H), 5.12 (s, 2H), 2.71 (s, 3H);  $^{13}\text{C NMR}$  (100 MHz,  $\text{CDCl}_3$ ): 164.07, 162.04, 157.24, 155.51, 134.07, 132.06, 129.19, 127.40, 122.72, 114.54, 113.85, 112.27, 102.09, 99.06, 70.13, 18.18; **IR** (ATR,  $\text{cm}^{-1}$ ): 3079, 2226, 1710, 1244, 657; **MS** (EI, 70 eV)  $m/z$ : 369.97  $[\text{M}+\text{H}]^+$ ; **HR-ESI**  $[\text{M}+\text{H}]^+$ : calcd. 370.0073, found. 370.0072.

#### 4.2.9. 7-[(4-Bromobenzyl)oxy]-4-(trifluoromethyl)-2H-chromen-2-one (9)

Yield: 65 % mp: 136 °C;  $^1\text{H NMR}$ : (400 MHz,  $\text{CDCl}_3$ )  $\delta_{\text{H}}$ : 7.66–7.64 (d, 1H,  $J = 8.8$  Hz), 7.56–7.52 (d, 2 H,  $J = 8.4$  Hz), 7.32–7.28 (d, 2H,  $J = 8.4$  Hz), 7.00–6.96 (dd, 1H,  $J = 8.8, 2.4$  Hz), 6.92–6.91 (m, 1H, H-8), 6.63 (s, 1H, H-3), 5.11 (s, 2H, H-15);  $^{13}\text{C NMR}$  (100 MHz,  $\text{CDCl}_3$ ): 162.22, 159.29, 156.23, 134.37, 132.00, 129.12, 126.49, 122.56, 113.91, 112.58, 112.52, 107.41, 102.42, 69.87; **IR** (ATR,  $\text{cm}^{-1}$ ): 3080, 1724, 1130, 657; **MS** (EI, 70 eV)  $m/z$ : 398.99  $[\text{M}+\text{H}]^+$ ; **HR-ESI**  $[\text{M}+\text{H}]^+$ : calcd. 398.9838, found. 398.9839.

#### 4.2.10. 7-[(4-Fluorobenzyl)oxy]-4-methyl-2-oxo-2H-chromene-3-carbonitrile (10)

Yield: 57%;  $^1\text{H NMR}$ : (400 MHz,  $\text{CDCl}_3$ )  $\delta_{\text{H}}$ : 7.68–7.66 (d, 1H,  $J = 9.1$  Hz), 7.56–7.43 (m, 2H), 7.15–7.10 (m, 2H), 7.05–7.00 (dd, 1H,  $J = 8.8, 2.4$  Hz), 6.90 (s, 1H), 5.15 (s, 2H), 2.74 (s, 3H); **MS** (EI, 70 eV)  $m/z$ : 310.10  $[\text{M}+\text{H}]^+$ ; **HR-ESI**  $[\text{M}+\text{H}]^+$ : calcd. 310.0874, found. 310.0876.

#### 4.2.11. 7-[(4-Chlorobenzyl)oxy]-4-methyl-2-oxo-2H-chromene-3-carbonitrile (11)

Yield: 82%;  $^1\text{H NMR}$ : (400 MHz,  $\text{CDCl}_3$ )  $\delta_{\text{H}}$ : 7.68–7.66 (d, 1H,  $J = 9.2$  Hz), 7.57–7.55 (d, 2H,  $J = 8.0$  Hz), 7.34–7.32 (d, 2H,  $J = 8.0$  Hz), 7.02–6.98 (dd, 1H,  $J = 8.8, 2.4$  Hz), 6.90 (s, 1H), 5.15 (s,

2H), 2.74 (s, 3H); MS (EI, 70 eV) m/z: 326.10 [M+H]<sup>+</sup>; HR-ESI [M+H]<sup>+</sup>: calcd. 326.0578, found. 326.0579.

#### 4.2.12. 7-[(3-Bromobenzyl)oxy]-4-methyl-2-oxo-2H-chromene-3-carbonitrile (12)

Yield: 76%; <sup>1</sup>H NMR: (400 MHz, CDCl<sub>3</sub>) δ<sub>H</sub>: 7.69–7.66 (d, 1H, J = 9.2 Hz), 7.61 (s, 1H) 7.57–7.54 (d, 1H, J = 8.0 Hz), 7.33–7.28 (m, 2H), 7.05–7.00 (dd, 1H, J = 8.8, 2.4 Hz), 6.90 (s, 1H), 5.12 (s, 2H), 2.71 (s, 3H); MS (EI, 70 eV) m/z: 369.98 [M+H]<sup>+</sup>; HR-ESI [M+H]<sup>+</sup>: calcd. 370.0073, found. 370.0074.

#### 4.2.13. 7-[(3,4-Dibromobenzyl)oxy]-4-methyl-2-oxo-2H-chromene-3-carbonitrile (13)

Yield: 76%; <sup>1</sup>H NMR: (400 MHz, DMSO) δ<sub>H</sub>: 7.95–7.92 (d, 1H, J = 9.3 Hz), 7.84–7.81 (d, 1H, J = 9.2 Hz), 7.77 (s, 1H), 7.42–7.38 (d, 1H, J = 8.0 Hz), 7.22–7.14 (m, 2H), 5.30 (s, 2H), 2.69 (s, 3H); MS (EI, 70 eV) m/z: 369.98 [M+H]<sup>+</sup>; HR-ESI [M+H]<sup>+</sup>: calcd. 370.0073, found. 370.0074.

### 4.2. General procedure for the synthesis of compounds 14 and 15

The appropriate commercially available 7-hydroxycoumarin (6.17 mmol, **1a** or **2a**) and K<sub>2</sub>CO<sub>3</sub> (12.33 mmol) were dissolved in 50 ml acetonitrile. To the mixture 1-(2-chloroethyl)piperidine hydrochloride (6.17 mmol) was added and stirred under reflux conditions at 80 °C for 3 hours, cooled down, filtered and evaporated to dryness. The remaining residue was extracted with 100 mL brine and 2 x 30 ml ethyl acetate. The combined organic fractions were dried over MgSO<sub>4</sub>, filtered and concentrated. Recrystallisation from EtOAc rendered compound **14** or **15** as yellow crystals.

#### 4.2.14. 7-[2-(Piperidin-1-yl)ethoxy]-2H-chromen-2-one (14)

Yield: 18.15 %; mp: 90 °C; <sup>1</sup>H NMR (600 MHz, CDCl<sub>3</sub>) δ<sub>H</sub>: 7.60 (d, 1H J = 9.5 Hz); 7.33 (d, 1H, J = 8.6 Hz); 6.82 (dd, 1H, J = 8.6, 2.4 Hz); 6.79 (d, 1H, J = 2.4 Hz); 6.21 (d, 1H, J = 9.5 Hz); 4.12 (t, 2H); 2.76 (t, 2H); 2.47 (s, 4H); 1.60 – 1.55 (m, 4H); 1.42 (s, 2H). <sup>13</sup>C NMR (150 MHz, CDCl<sub>3</sub>): 162.05; 161.21; 155.81; 143.38; 128.67; 113.03; 112.98; 112.50; 101.48; 66.63; 57.58; 55.06; 25.88; 24.09; HR-ESI [M+H]<sup>+</sup>: calcd. 274.1438, found. 274.1434.

#### 4.2.15. 4-Methyl-7-[2-(piperidin-1-yl)ethoxy]-2H-chromen-2-one (15)

Yield: 82.70 %; mp: 102–104 °C; <sup>1</sup>H NMR (600 MHz, CDCl<sub>3</sub>) δ<sub>H</sub>: 7.44 (d, 1H, J = 8.8 Hz), 6.82 (dd, 1H, J = 8.8, 2.4 Hz), 6.76 (d, 1H, J = 8.4 Hz), 6.08 (d, 1H, J = 8.4 Hz), 4.12 (t, 2H), 2.76 (t, 2H), 2.48 (s, 4H), 2.35 (m, 3H), 1.58 (m, 4H), 1.41 (s, 2H); <sup>13</sup>C NMR (150 MHz, CDCl<sub>3</sub>) 161.77; 161.23; 155.13; 152.48, 125.42, 113.52, 112.56, 111.85, 101.48, 66.44, 57.52, 55.00, 25.76, 24.00, 18.60; HR-ESI [M+H]<sup>+</sup>: calcd. 288.1594, found. 288.1593.

### 4.4. General procedure for the synthesis of compounds 16 – 25

A mixture of **1b–5b** (1 mmol) and 4-benzylpiperidine (1 mmol for compounds **16–20**) or 1-(4-bromobenzyl)piperazine (1 mmol for compounds **21–25**) in acetonitrile (10 mL) was refluxed in the presence of anhydrous  $K_2CO_3$  (1.1 mmol) for 8 h or until completion (monitored by TLC, mobile phase =  $CH_3Cl/MeOH$ , 50:1). After completion the reaction mixture was dried *in vacuo*, and the residue was purified by silica gel chromatography using  $CHCl_3/MeOH$  (50:1) as eluent to obtain compounds **16–25** as yellow oils.

#### 4.4.1. 7-[2-(4-Benzylpiperidin-1-yl)ethoxy]-2H-chromen-2-one (16)

Yield: 34 %;  $^1H$  NMR (400 MHz,  $CDCl_3$ )  $\delta_H$ : 7.67–7.63 (d, 1H, J = 9.6 Hz), 7.39–7.36 (d, 1H, J = 8.4 Hz), 7.32–7.28 (m, 1H), 7.23–7.15 (m, 4H), 6.88–6.84 (d, 1H, J = 8.8), 6.83 (s, 1H), 6.29–6.25 (d, 1H, J = 9.5 Hz), 4.17 (s, 2H), 3.02–2.99 (d, 2H, J = 10.6 Hz), 2.83 (s, 2H), 2.58–1.27 (m, 9H);  $^{13}C$  NMR (100 MHz,  $CDCl_3$ ): 162.02, 161.24, 155.83, 143.40, 140.54, 129.11, 128.67, 128.18, 125.82, 113.12, 112.99, 112.59, 101.52, 66.62, 57.18, 54.46, 43.12, 37.66, 32.03; IR (ATR,  $cm^{-1}$ ): 2922, 1729, 1610, 1124; MS (EI, 70 eV) m/z: 364.15  $[M+H]^+$ ; HR-ESI  $[M+H]^+$ : calcd. 364.1907, found. 364.1910.

#### 4.4.2. 4-Methyl-7-[2-(benzylpiperidine-1-yl)ethoxy]-2H-chromen-2-one (17)

Yield: 62 %  $^1H$  NMR: (400 MHz,  $CDCl_3$ )  $\delta_H$ : 7.48–7.45 (d, 1H, J = 8.8 Hz), 7.27–7.11 (m, 5H), 6.85–6.81 (dd, 1H, J = 8.8, 2.4 Hz), 6.79–6.77 (m, 1H), 6.12–6.11 (s, 1H), 4.15–4.12 (t, 2H), 3.00–2.96 (m, 2H), 2.82–2.78 (t, 2H), 2.54–2.51 (d, 2H, J = 7.04 Hz), 2.38–2.37 (s, 3H), 2.09–2.03 (t, 2H), 1.67–1.63 (d, 2H, J = 12.8 Hz), 1.57–1.50 (m, 1H), 1.40–1.29 (m, 2H);  $^{13}C$  NMR (100 MHz,  $CDCl_3$ ): 161.83, 155.23, 152.59, 140.56, 129.13, 128.20, 125.85, 125.50, 113.65, 112.69, 111.99, 101.55, 66.51, 57.23, 54.49, 43.13, 37.68, 32.01, 18.69; IR (ATR,  $cm^{-1}$ ): 3025, 2922, 1715, 1605, 1135; MS (EI, 70 eV) m/z: 378.19  $[M+H]^+$ ; HR-ESI  $[M+H]^+$ : calcd. 378.2064, found. 378.2059.

#### 4.2.3. 3-Chloro-4-methyl-7-[2-(benzylpiperidin-1-yl)ethoxy]-2H-chromen-2-one (18)

Yield: 30 %;  $^1H$  NMR (400 MHz,  $CDCl_3$ )  $\delta_H$ : 7.52–7.49 (d, 1H, J = 8.8 Hz), 7.29–7.25 (t, 2H), 7.21–7.18 (t, 1H, H=27), 7.15–7.12 (d, 2H, J = 7.2 Hz), 6.92–6.88 (dd, 1H, J = 9.2, 2.8 Hz), 6.82–6.80 (m, 1H), 4.16–4.12 (t, 2H), 2.99–2.95 (d, 2H, J = 12.8), 2.82–2.78 (t, 2H), 2.56–2.52 (d, 5H, J = 4.8 Hz), 2.10–2.02 (m, 2H), 1.67–1.63 (d, 2H, J = 12.8), 1.58–1.49 (m, 1H), 1.40–1.29 (m, 2H)  $^{13}C$  NMR (100 MHz,  $CDCl_3$ ): 161.82, 157.33, 753.10, 148.08, 140.41, 129.11, 128.17, 125.82, 113.37, 101.45, 66.68, 57.16, 54.49, 43.15, 37.66, 32.05, 16.16; IR (ATR,  $cm^{-1}$ ): 3070, 2930, 1719, 1600, 811; MS (EI, 70 eV) m/z: 412.16  $[M+H]^+$ ; HR-ESI  $[M+H]^+$ : calcd. 412.1674, found. 412.1673.

#### 4.2.4. 4-Methyl-2-oxo-7-[2-(benzylpiperidin-1-yl)-ethoxy]-2H-chromene-3-carbonitrile (19)

Yield: 56 %;  $^1H$  NMR (400 MHz,  $CDCl_3$ )  $\delta_H$ : 7.71–7.68 (d, 1H, J = 8.8 Hz), 7.38–7.20 (m, 5H), 7.05–7.02 (d, 1H, J = 8.8 Hz), 6.90 (s, 1H), 4.27 (s, 2H), 3.07–3.03 (d, 2H, J = 10.7 Hz), 2.89 (s, 2H), 2.80–2.79 (s, 3H), 2.64–2.61 (d, 2H, J = 6.7), 2.26–2.12 (t, 2H), 1.76–1.72 (d, 2H, J = 13.2 Hz),

1.63–1.62 (m, 1H), 1.47–1.33 (m, 2H);  $^{13}\text{C}$  NMR (100 MHz,  $\text{CDCl}_3$ ): 164.63, 162.07, 157.38, 155.56, 140.51, 129.10, 128.18, 127.20, 125.83, 114.41, 113.94, 111.93, 101.65, 98.69, 67.14, 57.05, 54.51, 43.09, 37.65, 32.03, 18.17; IR (ATR,  $\text{cm}^{-1}$ ): 3070, 2917, 1714, 1598; MS (EI, 70 eV)  $m/z$ : 403.21  $[\text{M}+\text{H}]^+$ ; HR-ESI  $[\text{M}+\text{H}]^+$ : calcd. 403.2016, found. 403.2020.

#### 4.2.5. 7-[2-(Benzylpiperidin-1-yl)ethoxy]-4-(trifluoromethyl)-2H-chromen-2-one (20)

Yield: 74 %;  $^1\text{H}$  NMR (400 MHz,  $\text{CDCl}_3$ )  $\delta_{\text{H}}$ : 7.26–7.12 (m, 6H), 6.94–6.90 (dd, 1H,  $J = 8.8, 2.4$  Hz), 6.88–6.86 (m, 1H), 6.61 (s, 1H), 4.18–4.14 (t, 2H), 2.98–2.94 (d, 2H,  $J = 2.4$  Hz), 2.82–2.79 (t, 2), 2.55–2.53 (d, 2H,  $J = 6.8$  Hz), 2.09–2.02 (t, 2H), 1.68–1.64 (d, 2H), 1.63–1.40 (m, 1H), 1.41–1.33 (m, 2H);  $^{13}\text{C}$  NMR (100 MHz,  $\text{CDCl}_3$ ): 140.53, 129.19, 128.11, 125.81, 113.71, 102.06, 66.96, 57.15, 54.54, 43.20, 37.68, 32.01; IR (ATR,  $\text{cm}^{-1}$ ): 3070, 1713, 1614, 1132; MS (EI, 70 eV)  $m/z$ : 432.23  $[\text{M}+\text{H}]^+$ ; HR-ESI  $[\text{M}+\text{H}]^+$ : calcd. 432.1781, found. 432.1785.

#### 4.2.6. 7-[2-[4-(4-Bromobenzyl)piperazin-1-yl]ethoxy]-2H-chromen-2-one (21)

Yield: 32 %;  $^1\text{H}$  NMR (400 MHz,  $\text{CDCl}_3$ )  $\delta_{\text{H}}$ : 7.63–7.60 (d, 1H,  $J = 9.6$  Hz), 7.43–7.40 (d, 2H,  $J = 8.4$  Hz), 7.36–7.33 (d, 1H,  $J = 8.6$  Hz), 7.20–7.17 (d, 2H,  $J = 8.4$  Hz), 6.84–6.81 (dd, 1H,  $J = 8.4, 2.4$  Hz), 6.80–6.79 (m, 1H), 6.25–6.22 (d, 1H,  $J = 9.6$  Hz), 4.16–4.12 (t, 2H), 3.44 (s, 2H), 2.85–2.81 (t, 2H, Hz), 2.61–2.48 (d, 8H,  $J = 48.0$  Hz);  $^{13}\text{C}$  NMR (100 MHz,  $\text{CDCl}_3$ ): 161.93, 161.17, 155.83, 143.34, 137.07, 131.32, 130.79, 128.71, 120.87, 113.17, 112.98, 112.61, 101.49, 66.52, 62.20, 56.81, 53.58, 52.86; IR (ATR,  $\text{cm}^{-1}$ ): 3072, 2944, 1729, 1614, 695; MS (EI, 70 eV)  $m/z$ : 443.15  $[\text{M}+\text{H}]^+$ ; HR-ESI  $[\text{M}+\text{H}]^+$ : calcd. 443.0965, found. 443.0971.

#### 4.2.7. 4-Methyl-7-[2-[4-(4-bromobenzyl)piperazin-1-yl]ethoxy]-2H-chromen-2-one (22)

Yield: 11 %;  $^1\text{H}$  NMR (400 MHz,  $\text{CDCl}_3$ )  $\delta_{\text{H}}$ : 7.49–7.46 (d, 1H,  $J = 8.8$  Hz), 7.44–7.41 (d, 2H,  $J = 8.4$  Hz), 7.21–7.18 (d, 2H,  $J = 8.4$  Hz), 6.87–6.84 (dd, 1H,  $J = 8.8, 2.4$  Hz), 6.81–6.80 (m, 1H), 6.12 (s, 1H), 4.17–4.13 (t, 2H), 3.45 (s, 2H), 2.86–2.82 (t, 2H,  $J = 5.6$  Hz), 2.62–2.49 (d, 7H,  $J = 47.2$  Hz), 7.38 (s, 3H);  $^{13}\text{C}$  NMR (100 MHz,  $\text{CDCl}_3$ ): 161.78, 161.34, 155.19, 152.55, 137.10, 131.33, 130.80, 125.54, 120.85, 113.68, 112.72, 111.99, 101.52, 66.48, 56.85, 53.62, 52.88, 18.68; IR (ATR,  $\text{cm}^{-1}$ ): 2938, 1610, 705; MS (EI, 70 eV)  $m/z$ : 457.17  $[\text{M}+\text{H}]^+$ ; HR-ESI  $[\text{M}+\text{H}]^+$ : calcd. 457.1121, found. 457.1121.

#### 4.2.8. 3-Chloro-4-methyl-7-[2-[4-(4-bromobenzyl)piperazine-1-yl]ethoxy]-2H-chromen-2-one (23)

Yield: 15 %;  $^1\text{H}$  NMR (400 MHz,  $\text{CDCl}_3$ )  $\delta_{\text{H}}$ : 7.52–7.48 (d, 1H,  $J = 8.8$  Hz), 7.44–7.41 (d, 2H,  $J = 8.4$  Hz), 7.21–7.17 (d, 2 H,  $J = 8.4$  Hz), 6.90–6.86 (dd, 1H,  $J = 9.2, 2.8$  Hz), 6.79–6.77 (m, 1H), 4.17–4.13 (t, 2H), 3.46 (s, 2H), 2.88–2.84 (t, 2H), 2.64–2.52 (m, 11H);  $^{13}\text{C}$  NMR (100 MHz,  $\text{CDCl}_3$ ): 161.77, 131.37, 130.86, 125.86, 113.22, 101.42, 66.81, 62.22, 56.80, 53.55, 52.73, 29.74;

**IR** (ATR,  $\text{cm}^{-1}$ ): 3395, 2923, 1601, 1002, 684; **MS** (EI, 70 eV)  $m/z$ : 491.14  $[\text{M}+\text{H}]^+$ ; **HR-ESI**  $[\text{M}+\text{H}]^+$ : calcd. 491.0732, found. 491.0733.

#### **4.2.9. 4-Methyl-2-oxo-7-[2-[4-(4-bromobenzyl)piperazin-1-yl]ethoxy]-2H-chromene-3-carbonitrile (24)**

Yield: 40 %;  **$^1\text{H}$  NMR** (400 MHz,  $\text{CDCl}_3$ )  $\delta_{\text{H}}$ : 7.62–7.58 (d, 1H,  $J = 8.8$  Hz), 7.43–7.40 (d, 2H,  $J = 8.4$  Hz), 7.20–7.17 (d, 2H,  $J = 8.4$  Hz), 6.96–6.92 (dd, 1H,  $J = 8.8, 2.4$  Hz), 6.82–6.80 (m, 1H), 4.19–4.16 (t, 2H), 3.44 (s, 2H), 2.89–2.75 (t, 2H), 2.69 (s, 3H), 2.54–2.47 (d, 8H,  $J = 23.2$  Hz);  **$^{13}\text{C}$  NMR** (100 MHz,  $\text{CDCl}_3$ ): 164.56, 162.04, 157.33, 155.59, 137.10, 131.35, 130.80, 127.23, 120.91, 114.40, 113.92, 112.00, 101.65, 98.80, 67.04, 62.22, 56.69, 53.65, 52.87, 18.14; **IR** (ATR,  $\text{cm}^{-1}$ ): 3071, 1720, 1007, 735; **MS** (EI, 70 eV)  $m/z$ : 482.20  $[\text{M}+\text{H}]^+$ ; **HR-ESI**  $[\text{M}+\text{H}]^+$ : calcd. 482.1074, found. 482.1079.

#### **4.2.10. 7-[2-[4-(4-Bromobenzyl)piperazin-1-yl]ethoxy]-4-(trifluoromethyl)-2H-chromen-2-one (25)**

Yield: 21 %;  **$^1\text{H}$  NMR**: (400 MHz,  $\text{CDCl}_3$ )  $\delta_{\text{H}}$ : 7.62–7.59 (d, 1 H,  $J = 9.2$  Hz), 7.44–7.41 (d, 2 H,  $J = 8.4$  Hz), 7.21–7.18 (d, 2H,  $J = 8.4$  Hz), 6.93–6.89 (dd, 1H,  $J = 9.2, 2.4$  Hz), 6.87–6.86 (m, 1H), 6.61 (s, 1H), 4.19–4.15 (t, 2H), 3.45 (s, 2H), 2.87–2.83 (t, 2H), 2.62–2.49 (m, 8H);  **$^{13}\text{C}$  NMR** (100 MHz,  $\text{CDCl}_3$ ): 131.35, 130.81, 113.73, 107.12, 102.10, 66.67, 62.19, 56.64, 53.61, 52.86; **IR** (ATR,  $\text{cm}^{-1}$ ): 2936, 2809, 1609, 1125, 1008; **MS** (EI, 70 eV)  $m/z$ : 511.14  $[\text{M}+\text{H}]^+$ ; **HR-ESI**  $[\text{M}+\text{H}]^+$ : calcd. 511.0839, found. 511.0840.

### **4.3. Recombinant human MAO-A and MAO-B inhibition studies**

The MAO assays were conducted using a similar procedure as previously described [48,49]. Recombinant human MAO-A and -B (5 mg/mL) were obtained from Sigma–Aldrich and were pre-aliquoted and stored at  $-70$  °C. All enzymatic reactions were carried out to a final volume of 250  $\mu\text{L}$  in potassium phosphate buffer (100 mM, pH 7.4, made isotonic with KCl, 20.2 mM) and contained kynuramine as substrate, MAO-A or MAO-B (0.0075 mg/mL) and various concentrations of the test inhibitor (0–1000  $\mu\text{M}$ ). The final concentrations of kynuramine in the reactions were 45  $\mu\text{M}$  and 30  $\mu\text{M}$  for MAO-A and -B, respectively. Stock solutions of the test inhibitors were prepared in DMSO and added to the reactions to yield a final concentration of 2% (v/v) DMSO. The reactions were incubated for 20 min at 37 °C and were terminated with the addition of 100  $\mu\text{L}$  NaOH (2 N). Finally 250  $\mu\text{L}$  from each eppendorf vial was added to individual black plate wells. The fluorescence of the MAO generated 4-hydroxyquinoline in the supernatant fractions were measured using a Biotek fluorescent microplate reader at an excitation wavelength of 310 nm and an emission wavelength of 400 nm.  $\text{IC}_{50}$  values were calculated as concentration of the compound that produces 50% enzyme activity inhibition, using the Graph Pad Prism 6 software (San Diego, CA, USA).

AChE from electric eel, BuChE from equine serum, S-butylthiocholine iodide (BTCI), acetylthiocholine iodide (ATCI), 5,5'-dithiobis-(2-nitrobenzoic acid) (Ellman's reagent, DTNB), donepezil and tacrine hydrochloride were purchased from Sigma-Aldrich. The inhibitory activities of test compounds **1 - 25** were evaluated by Ellman's method [50]. The compounds were dissolved in DMSO and diluted with the buffer solution (50 mM Tris-HCl, pH = 8.0) to yield the corresponding test concentrations (DMSO less than 0.01%). In each well of the plate, 160  $\mu$ L of 1.5 mM DTNB, 50  $\mu$ L of AChE (0.22 U/mL eeAChE) or 50  $\mu$ L of BuChE (0.12 U/mL eqBuChE) were incubated with 10  $\mu$ L of different concentrations of test compounds (0.01–100  $\mu$ M) at 37°C for 10 min. After this period, acetylthiocholine iodide (15 mM) or S-butyrylthiocholine iodide (15 mM) as the substrate (30  $\mu$ L) was added, incubated for a further 10 minutes, and thereafter the absorbance was measured at a wavelength of 405 nm at different time intervals (0, 60, 120, and 180 s). IC<sub>50</sub> values were calculated as concentration of the compound that produces 50% enzyme activity inhibition, using the Graph Pad Prism 6 software (San Diego, CA, USA).

#### **4.5. Molecular modeling studies**

##### **4.5.1. MAO docking studies**

Computer-assisted docking was carried out using the CHARMM force field and hMAO-A co-crystallized with harmine (PDB ID: 2Z5X) [53] and hMAO-B co-crystallized with 7-(3-chlorobenzoyloxy)-4-(methylamino)methyl-coumarin (PDB ID: 2V61) [43], which were recovered from the Brookhaven Protein Database ([www.rcsb.org/pdb](http://www.rcsb.org/pdb)). Docking simulations were performed on the test compounds using Molecular Operating Environment (MOE) [55] with the following protocol. (1) Enzyme structures were checked for missing atoms, bonds and contacts. (2) Hydrogens and partial charges were added using the protonate 3D application in MOE. (3) The ligands were constructed using the builder module and were energy minimized. (4) Ligands were docked within the MAO-A or MAO-B active sites using MOEDock application, the poses were generated by the Triangle Matcher placement method and were rescored using the ASE scoring function. (5) The retained best poses were visually inspected and the interactions with binding pocket residues were analyzed. To determine the accuracy of this docking protocol, the co-crystallised ligand, harmine (PDB ID: 2Z5X), was re-docked into the MAO-A active site and the co-crystallised ligand, 7-(3-chlorobenzoyloxy)-4-(methylamino)methyl-coumarin (PDB ID: 2V5Z), was re-docked into the MAO-B active site. This procedure was repeated three times and the best ranked solutions of harmine and 7-(3-chlorobenzoyloxy)-4-(methylamino)methyl-coumarin exhibited RMSD values of 0.42 Å and 0.62 Å from the position of the co-crystallised ligand for MAO-A and MAO-B, respectively. In general, RMSD values smaller than 2.0 Å, indicate that the docking protocol is capable of accurately predicting the binding orientation of the co-crystallised ligand [62,63]. These protocols were thus

deemed to be suitable for the docking of inhibitors into the active site models of MAO-A and MAO-B.

## 4.5.2. Cholinesterase docking studies

### 4.5.2.1. Acetylcholinesterase

The dock function of MOE [55] was used to predict the interactions and binding modes of the synthesized inhibitors in the eeAChE active site. The crystal structure of the eeAChE protein co-crystallized with donepezil was acquired from the Protein Data Bank (PDB ID: 1EVE) [54]. The docking procedure followed the same protocol as described for the MAO docking. To determine the accuracy of this docking protocol, the co-crystallised ligand, was re-docked into the AChE active site. This procedure was repeated three times and the best ranked solution exhibited an RMSD value of 1.15 Å from the position of the co-crystallised ligand. The RMSD value in this case is smaller than 2.0 Å indicating that the docking protocol is capable of accurately predicting the binding orientation of the co-crystallised ligand [62,63]. This protocol was thus deemed to be suitable for the docking of inhibitors into the active site model of AChE.

### 4.5.2.2. Butyrylcholinesterase

Because no X-ray structure exists for eqBuChE, a homology model was used to rationalize the experimental data. The eqBuChE model was retrieved from the SWISS-MODEL Repository. This is a database of annotated three-dimensional comparative protein structure models generated by the fully automated homology-modeling pipeline SWISS-MODEL. A putative three-dimensional structure of eqBuChE has been created based on the crystal structure of hBuChE (PDB ID: 2PM8), these two enzyme exhibited 89% sequence identity. Proper bonds, bond orders, hybridization and charges were assigned and CHARMM force field was applied using MOE [55]. The prepared protein was directly loaded into AutoDockTools (ADT; version 1.5.4), hydrogens were added and partial charges for proteins and ligands were calculated using Gasteiger charges. Flexible torsions in the ligands were assigned with the AutoTors module, and the acyclic dihedral angles were allowed to rotate freely. Docking calculations were performed with the program Autodock Vina [58]. Because VINA uses rectangular boxes for the binding site, the box center was defined and the docking box was displayed using ADT. All dockings were performed where a cube of 75 Å with grid points separated by 1 Å, was positioned over the active site of the protein (x = 29.885; y = -54.992; z = 58.141). Default parameters were used except num\_modes, which was set to 40. The lowest docking-energy conformation was considered as the most stable orientation. Finally, the docking results generated were analysed using MOE.

## Acknowledgements

We are grateful to the University of the Western Cape, North-West University and the National Research Foundation of South Africa for financial support.

## References

1. Goedert M, Spillantini M. A Century of Alzheimer's Disease. *Science* 2006; 314: 777-781.
2. Cummings J. The Dementias: Diagnosis, Treatment and Research, 3rd ed. *Arch Neurol* 2004; 61: 1623.
3. Grundke-Iqbal I, Iqbal K, Tung Y, Quinlan M, Wisniewski H, Binder L. Abnormal phosphorylation of the microtubule-associated protein tau (tau) in Alzheimer cytoskeletal pathology. *Proceedings of the National Academy of Sciences* 1986; 83: 4913-4917.
4. Castro A, Martinez A. Targeting Beta-Amyloid Pathogenesis Through Acetylcholinesterase Inhibitors. *CPD* 2006; 12: 4377-4387.
5. Gella A, Durany N. Oxidative stress in Alzheimer disease. *Cell Adhesion & Migration* 2009; 3: 88-93.
6. Coyle J, Puttfarcken P. Oxidative stress, glutamate, and neurodegenerative disorders. *Science* 1993; 262: 689-695.
7. Talesa V. Acetylcholinesterase in Alzheimer's disease. *Mechanisms of Ageing and Development* 2001; 122: 1961-1969.
8. Birks J, Harvey R. Donepezil for Dementia Due to Alzheimer's Disease. *Cochrane Database Syst. Rev.* 2006, No. 1, CD001190.
9. Loy C, Schneider L. Galantamine for Alzheimer's Disease. *Cochrane Database Syst. Rev.* 2004, No. 4, CD001747.
10. Birks J, Grimley E. J, Iakovidou V. Rivastigmine for Alzheimer's Disease. *Cochrane Database Syst. Rev.* 2000, No. 4, CD001191.
11. Greig N, Utsuki T, Ingram D, Wang Y, Pepeu G, Scali C et al. Selective butyrylcholinesterase inhibition elevates brain acetylcholine, augments learning and lowers Alzheimer B-amyloid peptide in rodent. *Proceedings of the National Academy of Sciences* 2005; 102: 17213-17218.
12. Giacobini E. Cholinergic function and Alzheimer's disease. *Int J Geriatr Psychiatry* 2003; 18: S1-S5.
13. Garcia-Alloza M, Gil-Bea F, Diez-Ariza M, Chen C, Francis P, Lasheras B et al. Cholinergic-serotonergic imbalance contributes to cognitive and behavioral symptoms in Alzheimer's disease. *Neuropsychologia* 2005; 43: 442-449.
14. Terry A, Buccafusco J, Wilson C. Cognitive dysfunction in neuropsychiatric disorders: Selected serotonin receptor subtypes as therapeutic targets. *Behavioural Brain Research* 2008; 195: 30-38.
15. Dringenberg H. Alzheimer's disease: more than a 'cholinergic disorder' — evidence that cholinergic-monoaminergic interactions contribute to EEG slowing and dementia. *Behavioural Brain Research* 2000; 115: 235-249.
16. Riederer P, Youdim M. Monoamine Oxidase Activity and Monoamine Metabolism in Brains of Parkinsonian Patients Treated with l-Deprenyl. *Journal of Neurochemistry* 1986; 46: 1359-1365.
17. Kristal S, Conway D, Brown M, Jain C, Ulluci A, Li W, Burke W. Selective dopaminergic vulnerability: 3,4-dihydroxyphenylacetaldehyde targets mitochondria. *Free Radical Biology and Medicine* 2001; 30: 924-931.
18. Mitoma J, Ito A. Mitochondrial targeting signal of rat liver monoamine oxidase B is located at its carboxy terminus. *Journal of Biochemistry.* 1992; 111: 20-24.
19. Greenawalt J. An appraisal of the use of monoamine oxidase as an enzyme marker for the outer membrane of rat liver mitochondria. *The Journal of Cell Biology* 1970; 46: 173-179.
20. Johnston J. Some observations upon a new inhibitor of monoamine oxidase in brain tissue. *Biochemical Pharmacology* 1968; 17: 1285-1297.
21. Youdim M, Edmondson D, Tipton K. The therapeutic potential of monoamine oxidase inhibitors. *Nature Reviews Neuroscience* 2006; 7: 295-309.
22. Pizzinat N, Copin N, Vindis C, Parini A, Cambon C. Reactive oxygen species production by monoamine oxidases in intact cells. *Naunyn-Schmiedeberg's Archives of Pharmacology* 1999; 359: 428-431.
23. Danielczyk W, Streifler M, Konradi C, Riederer P, Moll G. Platelet MAO-B activity and the psychopathology of Parkinson's disease, senile dementia and multi-infarct dementia. *Acta Psychiatrica Scandinavica* 1988; 78: 730-736.
24. Cai Z. Monoamine oxidase inhibitors: Promising therapeutic agents for Alzheimer's disease (Review). *Molecular Medicine Reports* 2014. doi:10.3892/mmr.2014.2040.
25. Vishnu Nayak B, Ciftci-Yabanoglu S, Jadav S, Jagrat M, Sinha B, Ucar G et al. Monoamine oxidase inhibitory activity of 3,5-biaryl-4,5-dihydro-1H-pyrazole-1-carboxylate derivatives. *European Journal of Medicinal Chemistry* 2013; 69: 762-767.
26. Filip E, Kolibas. Selegiline in the treatment of Alzheimer's disease: a long-term randomized placebo-controlled trial. Czech and Slovak Senile Dementia of Alzheimer Type Study Group. *Journal Psychiatry and Neuroscience* 1999; 24: 234-243.
27. Joubert J, Petzer J, Prins L, Repsold B, Malan S. Multifunctional enzyme inhibition for neuroprotection -0 A focus on MAO, NOS and AChE inhibitors. In *Drug Design and Discovery in Alzheimer's Disease*; Bentham Books, 2014; pp. 291-365.

28. Cavalli A, Bolognesi M, Minarini A, Rosini M, Tumiatti V, Recanatini M et al. Multi-target-Directed Ligands To Combat Neurodegenerative Diseases. *Journal of Medicinal Chemistry* 2008; 51: 347-372.
29. Youdim M, Buccafusco J. Multi-functional drugs for various CNS targets in the treatment of neurodegenerative disorders. *Trends in Pharmacological Sciences* 2005; 26: 27-35.
30. Brühlmann C, Ooms F, Carrupt P, Testa B, Catto M, Leonetti F et al. Coumarins Derivatives as Dual Inhibitors of Acetylcholinesterase and Monoamine Oxidase. *J Med Chem* 2001; 44: 3195-3198.
31. Sterling J, Herzig Y, Goren T, Finkelstein N, Lerner D, Goldenberg W et al. Novel Dual Inhibitors of AChE and MAO Derived from Hydroxy Aminoindan and Phenethylamine as Potential Treatment for Alzheimer's Disease. *Journal of Medicinal Chemistry* 2002; 45: 5260-5279.
32. Pisani L, Catto M, Leonetti F, Nicolotti O, Stefanachi A, Campagna F et al. Targeting Monoamine Oxidases with Multipotent Ligands: An Emerging Strategy in the Search of New Drugs Against Neurodegenerative Diseases. *Current Medicinal Chemistry* 2011; 18: 4568-4587.
33. Bolea I, Juárez-Jiménez J, de los Ríos C, Chioua M, Pouplana R, Luque F et al. Synthesis, Biological Evaluation, and Molecular Modeling of Donepezil and N -[(5-(Benzyloxy)-1-methyl-1 H -indol-2-yl)methyl]- N -methylprop-2-yn-1-amine Hybrids as New Multipotent Cholinesterase/Monoamine Oxidase Inhibitors for the Treatment of Alzheimer's Disease. *Journal of Medicinal Chemistry* 2011; 54: 8251-8270.
34. Samadi A, de los Ríos C, Bolea I, Chioua M, Iriepa I, Moraleda I et al. Multipotent MAO and cholinesterase inhibitors for the treatment of Alzheimer's disease: Synthesis, pharmacological analysis and molecular modeling of heterocyclic substituted alkyl and cycloalkyl propargyl amine. *European Journal of Medicinal Chemistry* 2012; 52: 251-262.
35. Yanez M, Vina D. Dual Inhibitors of Monoamine Oxidase and Cholinesterase for the Treatment of Alzheimer Disease. *CTMC* 2013; 13: 1692-1706.
36. Bautista-Aguilera O, Samadi A, Chioua M, Nikolic K, Filipic S, Agbaba D et al. N -Methyl- N -((1-methyl-5-(3-(1-(2-methylbenzyl)piperidin-4-yl)propoxy)-1 H -indol-2-yl)methyl)prop-2-yn-1-amine, a New Cholinesterase and Monoamine Oxidase Dual Inhibitor. *Journal of Medicinal Chemistry* 2014; 57: 10455-10463.
37. Wang L, Esteban G, Ojima M, Bautista-Aguilera O, Inokuchi T, Moraleda I et al. Donepezil + propargylamine + 8-hydroxyquinoline hybrids as new multifunctional metal-chelators, ChE and MAO inhibitors for the potential treatment of Alzheimer's disease. *European Journal of Medicinal Chemistry* 2014; 80: 543-561.
38. Farina R, Pisani L, Catto M, Nicolotti O, Gadaleta D, Denora N et al. Structure-Based Design and Optimization of Multitarget-Directed 2 H -Chromen-2-one Derivatives as Potent Inhibitors of Monoamine Oxidase B and Cholinesterases. *Journal of Medicinal Chemistry* 2015; 58: 5561-5578.
39. Xie S, Lan J, Wang X, Wang Z, Jiang N, Li F et al. Design, synthesis and biological evaluation of novel donepezil-coumarin hybrids as multi-target agents for the treatment of Alzheimer's disease. *Bioorganic & Medicinal Chemistry* 2016; 24: 1528-1539.
40. Patil P, Bari S, Firke S, Deshmukh P, Donda S, Patil D. A comprehensive review on synthesis and designing aspects of coumarin derivatives as monoamine oxidase inhibitors for depression and Alzheimer's disease. *Bioorganic & Medicinal Chemistry* 2013; 21: 2434-2450.
41. Gnerre C, Catto M, Leonetti F, Weber P, Carrupt P, Altomare C et al. Inhibition of Monoamine Oxidases by Functionalized Coumarin Derivatives: Biological Activities, QSARs, and 3D-QSARs. *Journal of Medicinal Chemistry* 2000; 43: 4747-4758.
42. Pisani L, Muncipinto G, Miscioscia T, Nicolotti O, Leonetti F, Catto M et al. Discovery of a Novel Class of Potent Coumarin Monoamine Oxidase B Inhibitors: Development and Biopharmacological Profiling of 7-[(3-Chlorobenzyl)oxy]-4-[(methylamino)methyl]-2H-chromen-2-one Methanesulfonate (NW-1772) as a Highly Potent, Selective, Reversible, and Orally Active Monoamine Oxidase B Inhibitor. *Journal of Medicinal Chemistry* 2009; 52: 6685-6706.
43. Binda C, Wang J, Pisani L, Caccia C, Carotti A, Salvati P et al. Structures of Human Monoamine Oxidase B Complexes with Selective Noncovalent Inhibitors: Saffinamide and Coumarin Analogs. *Journal of Medicinal Chemistry* 2007; 50: 5848-5852.
44. Inestrosa N, Alvarez A, Pérez C, Moreno R, Vicente M, Linker C et al. Acetylcholinesterase Accelerates Assembly of Amyloid- $\beta$ -Peptides into Alzheimer's Fibrils: Possible Role of the Peripheral Site of the Enzyme. *Neuron* 1996; 16: 881-891.
45. De Ferrari G, Canales M, Shin I, Weiner L, Silman I, Inestrosa N. A Structural Motif of Acetylcholinesterase That Promotes Amyloid  $\beta$ -Peptide Fibril Formation. *Biochemistry* 2001; 40: 10447-10457.
46. Rees T, Berson A, Sklan E, Younkin L, Younkin S, Brimijoin S et al. Memory Deficits Correlating with Acetylcholinesterase Splice Shift and Amyloid Burden in Doubly Transgenic Mice. *CAR* 2005; 2: 291-300.
47. Dinamarca M, Sagal J, Quintanilla R, Godoy J, Arrázola M, Inestrosa N. Amyloid- $\beta$ -Acetylcholinesterase complexes potentiate neurodegenerative changes induced by the A $\beta$  peptide. Implications for the pathogenesis of Alzheimer's disease. *Molecular Neurodegeneration* 2010; 5: 4.
48. Novaroli L, Reist M, Favre E, Carotti A, Catto M, Carrupt P. Human recombinant monoamine oxidase B as reliable and efficient enzyme source for inhibitor screening. *Bioorganic & Medicinal Chemistry* 2005; 13: 6212-6217.
49. Tavari M, Malan S, Joubert J. Design, synthesis, biological evaluation and docking studies of sulfonyl isatin derivatives as monoamine oxidase and caspase-3 inhibitors. *Med Chem Commun* 2016. doi:10.1039/c6md00228e.
50. Ellman G, Courtney K, Andres V, Featherstone R. A new and rapid colorimetric determination of

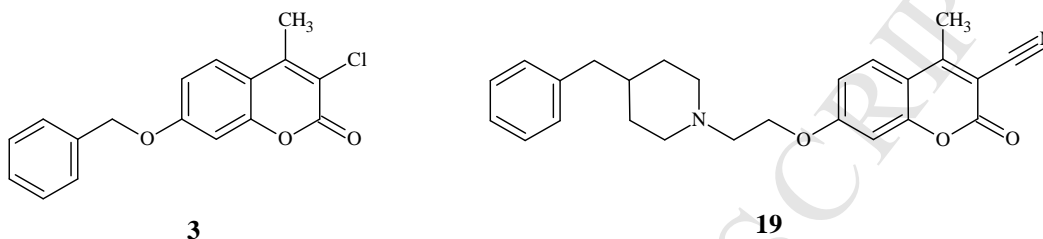
acetylcholinesterase activity. *Biochemical Pharmacology* 1961; 7: 88-95.

51. Meng F, Mao F, Shan W, Qin F, Huang L, Li X. Design, synthesis, and evaluation of indanone derivatives as acetylcholinesterase inhibitors and metal-chelating agents. *Bioorganic & Medicinal Chemistry Letters* 2012; 22: 4462-4466.
52. Sugimoto H, Ogura H, Arai Y, Iimura Y, Yamanishi Y. Research and Development of Donepezil Hydrochloride, a New Type of Acetylcholinesterase Inhibitor. *The Japanese Journal of Pharmacology* 2002; 89: 7-20.
53. Son, S.; Ma, J.; Kondou, Y.; Yoshimura, M.; Yamashita, E.; Tsukihara, T. *Proceedings of the National Academy of Sciences* 2008, 105, 5739-5744.
54. Kryger G, Silman I, Sussman J. Structure of acetylcholinesterase complexed with E2020 (Aricept®): implications for the design of new anti-Alzheimer drugs. *Structure* 1999; 7: 297-307.
55. Molecular Operating Environment (MOE), Version 2015.10. <http://www.chemcomp.com>.
56. Arnold K, Bordoli L, Kopp J, Schwede T. The SWISS-MODEL workspace: a web-based environment for protein structure homology modelling. *Bioinformatics* 2005; 22: 195-201.
57. Kiefer F, Arnold K, Kunzli M, Bordoli L, Schwede T. The SWISS-MODEL Repository and associated resources. *Nucleic Acids Research* 2009; 37: D387-D392.
58. Trott Olson A. AutoDock Vina: Improving the speed and accuracy of docking with a new scoring function, efficient optimization, and multithreading. *Journal of Computational Chemistry* 2009; 31: 455-461.
59. Bajda M, Więckowska A, Hebda M, Guzior N, Sottriffer C, Malawska B. Structure-Based Search for New Inhibitors of Cholinesterases. *IJMS* 2013; 14: 5608-5632.
60. Venneri A, McGeown W, Shanks M. Empirical evidence of neuroprotection by dual cholinesterase inhibition in Alzheimers disease. *NeuroReport* 2005; 16: 107-110.
61. Giacobini E. Cholinesterase inhibitors: new roles and therapeutic alternatives. *Pharmacological Research* 2004; 50: 433-440
62. Binda C, Li M, Hubalek F, Restelli N, Edmondson D, Mattevi A. Insights into the mode of inhibition of human mitochondrial monoamine oxidase B from high-resolution crystal structures. *Proceedings of the National Academy of Sciences* 2003; 100: 9750-9755.
63. Boström J, Greenwood J, Gottfries J. Assessing the performance of OMEGA with respect to retrieving bioactive conformations. *Journal of Molecular Graphics and Modelling* 2003; 21: 449-462.

## Synthesis and evaluation of 7-substituted coumarin derivatives as multimodal monoamine oxidase-B and cholinesterase inhibitors for the treatment of Alzheimer's disease

Jacques Joubert<sup>a,\*</sup>, Germaine B. Foka<sup>a</sup>, Benjamin P. Repsold<sup>b</sup>, Douglas W. Oliver<sup>b</sup>, Erika Kapp<sup>a</sup>, Sarel Malan<sup>a</sup>

<sup>a</sup>Pharmaceutical Chemistry, School of Pharmacy, University of the Western Cape, Private Bag X17, Bellville, South Africa. <sup>b</sup>School of Pharmacy, North-West University, Private Bag X6001, Potchefstroom, South Africa



Compound	IC <sub>50</sub> (μM) hMAO-A	IC <sub>50</sub> (μM) hMAO-B	IC <sub>50</sub> (μM) eeAChE	IC <sub>50</sub> (μM) eqBuChE
<b>3</b>	2.13	0.0021	>100	0.96
<b>19</b>	>10	0.30	9.10	5.90

- Twenty-five 7-substituted coumarin derivatives were successfully synthesised and evaluated.
- Compound **3** showed potent and selective MAO-B and BuChE inhibitory activity.
- Compound **19** was able to inhibit MAO-B, AChE and BuChE in the  $\mu\text{M}$  range.
- Docking revealed that **19** binds simultaneously to the CAS and PAS sites of AChE.
- It is suggested that **19** will be able to inhibit AChE induced A $\beta$  aggregation.

**Figure 1:** Design strategy for the 7-substituted coumarins incorporating different portions and distinct variations of the *N*-benzylpiperidine moiety of donepezil.

**Figure 2:** Synthetic pathway for the synthesis of compounds **1 – 15**.

**Figure 3:** Synthetic pathway for the synthesis of compounds **16 - 25**.

**Figure 4:** The hMAO-B active site cavity (left) and interaction maps (right) displaying the binding and interactions of compounds **3** (top) and **19** (bottom). FAD is shown in red and the compounds are shown in green in the active site cavity.

**Figure 5:** The eeAChE active site cavity (left) and interaction map (right) displaying the binding and interactions of compounds of **3** (top) and **19** (bottom).

**Figure 6:** Complex of compound **3** (top) and **19** (bottom) with the eqBuChE homology model (left) and the interaction maps (right).

**Table 1:** *In vitro* IC<sub>50</sub> values of test compounds **1-15** for hMAO-A, hMAO-B, eeAChE and eqBuChE.